

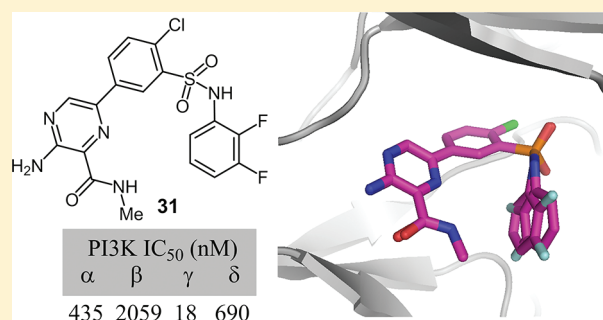
Discovery of a Novel Series of Potent and Orally Bioavailable Phosphoinositide 3-Kinase γ Inhibitors

James W. Leahy, Chris A. Buhr, Henry W. B. Johnson,* Byung Gyu Kim, TaeGon Baik, Jonah Cannoy, Timothy P. Forsyth, Joon Won Jeong, Matthew S. Lee, Sunghoon Ma, Kevin Noson, Longcheng Wang, Matthew Williams, John M. Nuss, Eric Brooks, Paul Foster, Leanne Goon, Nathan Heald, Charles Holst, Christopher Jaeger, Scott Lam, Julie Lougheed, Lam Nguyen, Arthur Plonowski, Joanne Song, Thomas Stout, Xiang Wu, Michael F. Yakes, Peiwen Yu, Wentao Zhang, Peter Lamb, and Olivia Raeber

Department of Drug Discovery, Exelixis, 169 Harbor Way, South San Francisco, California 94083, United States

S Supporting Information

ABSTRACT: The phosphoinositide 3-kinases (PI3Ks) have been linked to an extraordinarily diversified group of cellular functions making these enzymes compelling targets for the treatment of disease. A large body of evidence has linked PI3K γ to the modulation of autoimmune and inflammatory processes making it an intriguing target for drug discovery. Our high-throughput screening (HTS) campaign revealed two hits that were nominated for further optimization studies. The in vitro activity of the first HTS hit, designated as the sulfonylpiperazine scaffold, was optimized utilizing structure-based design. However, nonoptimal pharmacokinetic properties precluded this series from further studies. An overlay of the X-ray structures of the sulfonylpiperazine scaffold and the second HTS hit within their complexes with PI3K γ revealed a high degree of overlap. This feature was utilized to design a series of hybrid analogues including advanced leads such as **31** with desirable potency, selectivity, and oral bioavailability.



INTRODUCTION

The phosphoinositide 3-kinases (PI3Ks) are attractive targets for the design of small molecule inhibitors since abnormal PI3K activity contributes to the transition from typical cell function to the progression of disease.^{1–5} The most extensively studied of the three PI3K classes, class I, includes heterodimeric proteins consisting of a catalytic subunit (p110 α , p110 β , p110 δ , and p110 γ) and regulatory subunit (p85 in the case of p110 α , p110 β , and p110 δ ; either p84 or p101 in the case of PI3K γ).⁵ This target is further grouped into the class IA subset, comprising PI3K α , β , and δ , which is predominately activated by receptor tyrosine kinase signaling and the lone class IB member, PI3K γ , which is activated by G-protein coupled receptors.^{1,6–9}

The primary role of the class I PI3Ks involves catalyzing the phosphorylation of phosphatidylinositol (3,4)-bisphosphate (PIP2) to phosphatidylinositol (3,4,5)-triphosphate (PIP3).⁴ However, despite this unifying characteristic, differences in tissue distribution among the isoforms allows for differentiation in a disease setting. Where PI3K α and PI3K β are ubiquitously expressed, PI3K δ and PI3K γ expression is restricted primarily to the hematopoietic system.^{6–11} The class IA PI3Ks regulate many diverse processes and have been studied extensively as targets for the treatment of cancer and metabolic disorders.^{12,13} Experimental evidence has uncovered the link between PI3K γ and processes such as lymphocyte chemotaxis and mast cell

degranulation, thereby generating interest in this target for the treatment of autoimmune and inflammatory disorders.^{14–16} Recently, several reports linking PI3K γ to cancer,^{17–21} diabetes,²² cardiovascular disease,^{23–28} and Alzheimer's²⁹ have also been disclosed.

Given the overwhelming evidence linking the PI3K pathway to various disease states, there have been reports from a number of research groups targeting both pan-active and isoform selective inhibitors. These efforts have resulted in a considerable number of compounds now in the clinic, two of which were generated by our in-house program.³⁰ Both agents are pan-active inhibitors of the class I PI3Ks and are differentiated primarily by their activity against the closely related PIKK family member mTOR.^{31,32} Our more recent exploration has involved targeting isoform selective inhibitors in attempts to deconvolute the pharmacological activity observed with pan-active PI3K inhibition.

Fortunately, at the start of our work several reports exploring the potential of selective PI3K γ and dual PI3K γ / δ inhibition as a target profile for the treatment of inflammatory disease existed.^{33–35} Collectively, this large body of evidence provided a therapeutic rationale for pursuing PI3K γ as a drug discovery target and alleviated concerns around the risk of inhibiting this

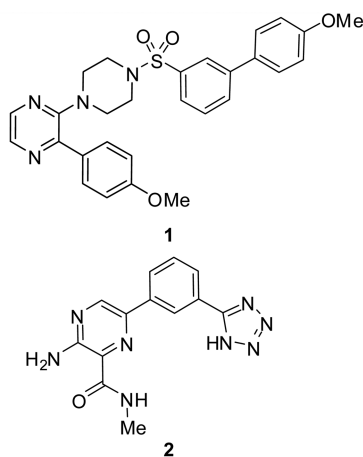
Received: March 22, 2012

Published: May 1, 2012

central signaling enzyme. The premise that PI3K γ inhibition would cause undesired side effects as a consequence of down-regulating central signaling pathways, such as mitogen-activated protein kinase (MAPK),^{36–39} was largely addressed by knockout and knock-in studies which indicated that mice lacking PI3K γ activity are viable and fertile.^{40–42} Subsequently, a groundbreaking report from Camps and co-workers disclosed the first PI3K γ selective inhibitor which demonstrated the role of pharmacological inhibition on this target in a disease setting.⁴³ In addition to this disclosure, few other examples of subtype selective PI3K γ inhibitors have been disclosed.^{33,44} In an effort to further investigate the role of PI3K γ in autoimmune and inflammatory disorders, we embarked on a campaign to design a tool compound with selectivity for PI3K γ vs class IA isoforms (PI3K α , β , and δ) and pharmacokinetic properties amenable to oral dosing. Herein is described our efforts to this end.

RESULTS AND DISCUSSION

Screening of our extensive ~4.6 million compound in-house library revealed hits **1** and **2** that we felt could be useful starting points from which to initialize lead optimization studies (Figure 1).



	1	2
PI3K γ IC ₅₀ (nM)	441	21
PI3K selectivity		
α	960	529
β	>10,000	6201
δ	1134	4204
cell IC ₅₀ (nM)	3608	>10,000
mouse plasma exposure ^{a, b}	0.5 ± 0.02 μ M (1 h) 0.1 ± 0.2 μ M (4 h)	n.d.

^aFemale athymic nude mice (n = 3) dosed at 100 mpk (PO) as a suspension in saline + HCl. Data reported as the mean ± SD

^bn.d. = not determined

Figure 1. Data for HTS hits **1** and **2**.

Assessment of biochemical selectivity was carried out with a luciferase-coupled chemiluminescence assay. Compounds were evaluated in a cellular context by measuring inhibition of AKT (PKB) phosphorylation with C5a-stimulated Raw 264.7 murine macrophages in a fixed-cell ELISA format.⁴³ HTS hit **1** possessed moderate in vitro potency and poor selectivity for PI3K γ vs α , β , and δ . Further evaluation of the pharmacokinetic profile of **1** demonstrated that a <1 μ M concentration was

observed in the plasma when dosed orally in mice at 100 mpk after one and four hours. The second HTS hit **2** was previously prepared as part of a program aimed at the inhibition of checkpoint kinases 1 and 2.⁴⁵ While **2** was not particularly active in these investigations, its biochemical and selectivity profile against PI3K γ was noteworthy. Given that the IC₅₀ of **2** was >10 μ M when tested in our cellular assay, we chose to prioritize our optimization efforts on **1** with the knowledge that **2** could serve as a viable scaffold as well.

The first generation of analogues aimed at improving the potency and selectivity of **1** utilized key observations gathered from a cocrystal structure of the ligand bound to the ATP-binding site of PI3K γ (Figure 2). Interaction of **1** with the

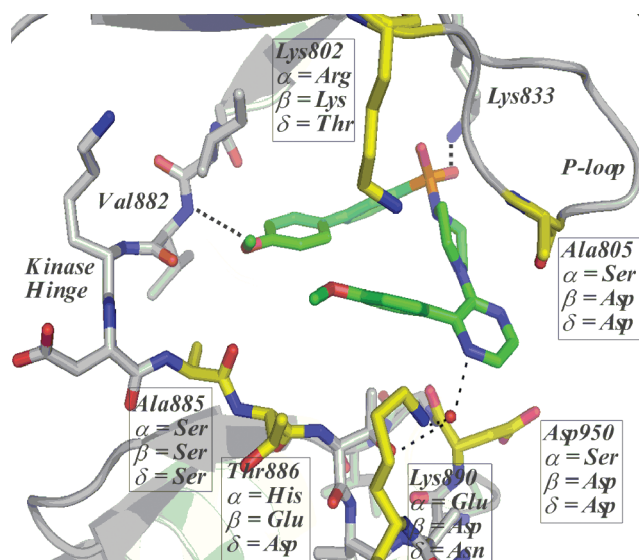
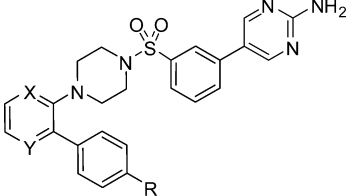


Figure 2. Cocrystal structure of **1** in the PI3K γ active site (PDB code 4anv). Residues nearest **1** in the PI3K γ active site that are different among class I PI3K isoforms are displayed in yellow. Hydrogen bonds of **1** with Val882 and Lys833 are illustrated.

PI3K γ hinge occurs through hydrogen bonding of the methoxy phenyl oxygen to the backbone NH of Val882; a fact that was not surprising based on the significant number of ligands that engage oxygen with this residue.⁴⁶ From our structural data, it appeared likely that converting the methoxyphenyl group interacting with Val882 to a functional group capable of forming a bidentate interaction would improve the PI3K activity. Indeed, introduction of the aminopyrimidine, with analogue **3**, produced a >40-fold improvement in biochemical activity for PI3K γ (Table 1). A high degree of homology is exhibited within the class I PI3Ks; therefore, to improve γ selectivity priority was given to modifying a part of the scaffold in close proximity to a less conserved region along the periphery of the active site.⁴⁷ Selectivity residues near the ligand are highlighted in Figure 2. The effectiveness of this strategy was exemplified with modification of the R group of **3**, where replacing the methoxy group with an isopropyl group, to provide **4**, improved the PI3K selectivity in favor of γ over α and β (Table 1). Unfortunately, **4** displayed poor plasma exposure in mice, presumably due to high mouse liver microsome (MLM) oxidation (79 ± 2.6% conversion at 30 min). Pyridine **5** displayed lower mouse liver microsome oxidation (37 ± 2.7% conversion at 30 min) and in-turn higher mouse plasma exposure than pyrazine **4**. However, despite

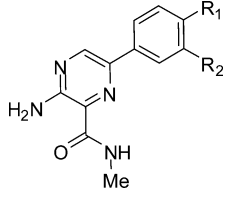
Table 1. Optimization of Sulfonylpiperazine Derivatives of HTS Hit 1

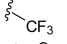
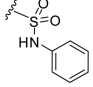
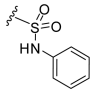


compd	X	Y	R	PI3K γ IC ₅₀ (nM)	PI3K γ cell IC ₅₀ (nM)	PI3K selectivity IC ₅₀ (nM)			mouse plasma exposure ^{a,b}	rat PK ^{b,c}
						α	β	δ		
3	N	N	OMe	10	264	38	1970	387	n.d.	n.d.
4	N	N	iPr	18	182	505	>10,000	816	0.7 ± 0.3 μ M (1 h) ^d 0.1 ± 0.08 μ M (4 h) ^d	n.d.
5	C	N	iPr	18	213	220	3512	456	12.9 ± 1.4 μ M (1 h) ^e 3.2 ± 0.9 μ M (4 h) ^e	AUC _(0-∞) = 0.95 μ M•h, t _{1/2} = 1.82 h, %F = 12.7

^aData are reported as the mean ± SD. ^bn.d. = not determined. ^cFemale Sprague–Dawley rats ($n = 3$) dosed at 5 mpk (PO) as a solution in 5% EtOH 45% PEG400/water + 1:2 HCl. ^dMale C57BL6 mice ($n = 3$) dosed at 100 mpk (PO) as a suspension in 0.5% CMC 0.2% Tween80/water. ^eMale C57BL6 mice ($n = 3$) dosed at 100 mpk (PO) as a turbid solution in 10% EtOH 20% PEG400/water + 1:1 HCl.

Table 2. In Vitro Potency and Selectivity Data for Derivatives of HTS Hit 2



compd	R ₁	R ₂	PI3K γ IC ₅₀ (nM)	PI3K γ Cell IC ₅₀ (nM)	PI3K selectivity IC ₅₀ (nM)		
					α	β	δ
6	H		777	5430	3575	>10,000	8359
7	H		60	326	744	2970	1095
8	Cl		39	69	174	578	352

other efforts to improve the pharmacokinetics of the sulfonyl piperazine series, **5** was our most promising analogue thus far. The combination of moderate mouse plasma exposure along with undesirable rat pharmacokinetic properties precluded further evaluation of this analogue. When considering the poor oral bioavailability of **5**, the low solubility ($K_{sol} < 5 \mu\text{M}$) was considered a primary factor. As the analogues in this series had high molecular weight (>500) and lipophilicity ($\text{LogD}_{7.4} > 4.0$),⁴⁸ lowering these values was viewed as an attractive approach to improving the solubility.

Fortunately, HTS hit **2** had considerably higher solubility ($K_{sol} = 424 \mu\text{M}$), lower lipophilicity ($\text{LogD}_{7.4} = 0.47$), and molecular weight (MW = 296). Therefore, **2** seemed like a more reasonable starting point for pharmacokinetic optimization since solubility would not likely be a limiting factor in achieving acceptable oral bioavailability in this series. In the optimization of **2**, our first priority was improving the poor cellular activity ($\text{IC}_{50} > 10 \mu\text{M}$), and there was evidence to infer this could be addressed by replacement of the tetrazole functional group. For example, lower biochemical activity, yet increased cellular activity, was observed when the tetrazole was replaced with a trifluoromethyl group (**6**, Table 2). Fortunately,

our optimization effort was aided by structural data of HTS hit **2** and sulfonyl piperazine **4**.

An overlay of the cocrystal structures of **2** and **4** indicated that these analogues adopted a similar binding mode (Figure 3). With **4**, hydrogen bonding with kinase hinge residue Val882 involved the aminopyrimidine, and with **2**, a similar interaction is formed with the aminopyrazine. Additionally, interaction with the salt bridge residue Lys833 occurs via the tetrazole of **2** and the sulfonamide oxygen of **4**. Therefore, when considering a surrogate functional group for the tetrazole, a sulfonamide was deemed appropriate since it would be able to interact with Lys833 while also allowing for additional structural manipulation. It was also deemed beneficial that the tetrazole of **2** did not reside in close proximity to selectivity residues within the active site, and therefore, modifying this region would be less likely to disrupt the desirable PI3K γ selectivity of this analogue.

Described in Table 2 is a representative sample of our initial attempts to find a suitable sulfonamide replacement for the tetrazole of **2**. Phenylsulfonamide **7** displayed a similar biochemical potency and selectivity profile to **2**, but with greatly enhanced cellular activity, thereby providing evidence that the potency would be retained with an appropriate tetrazole

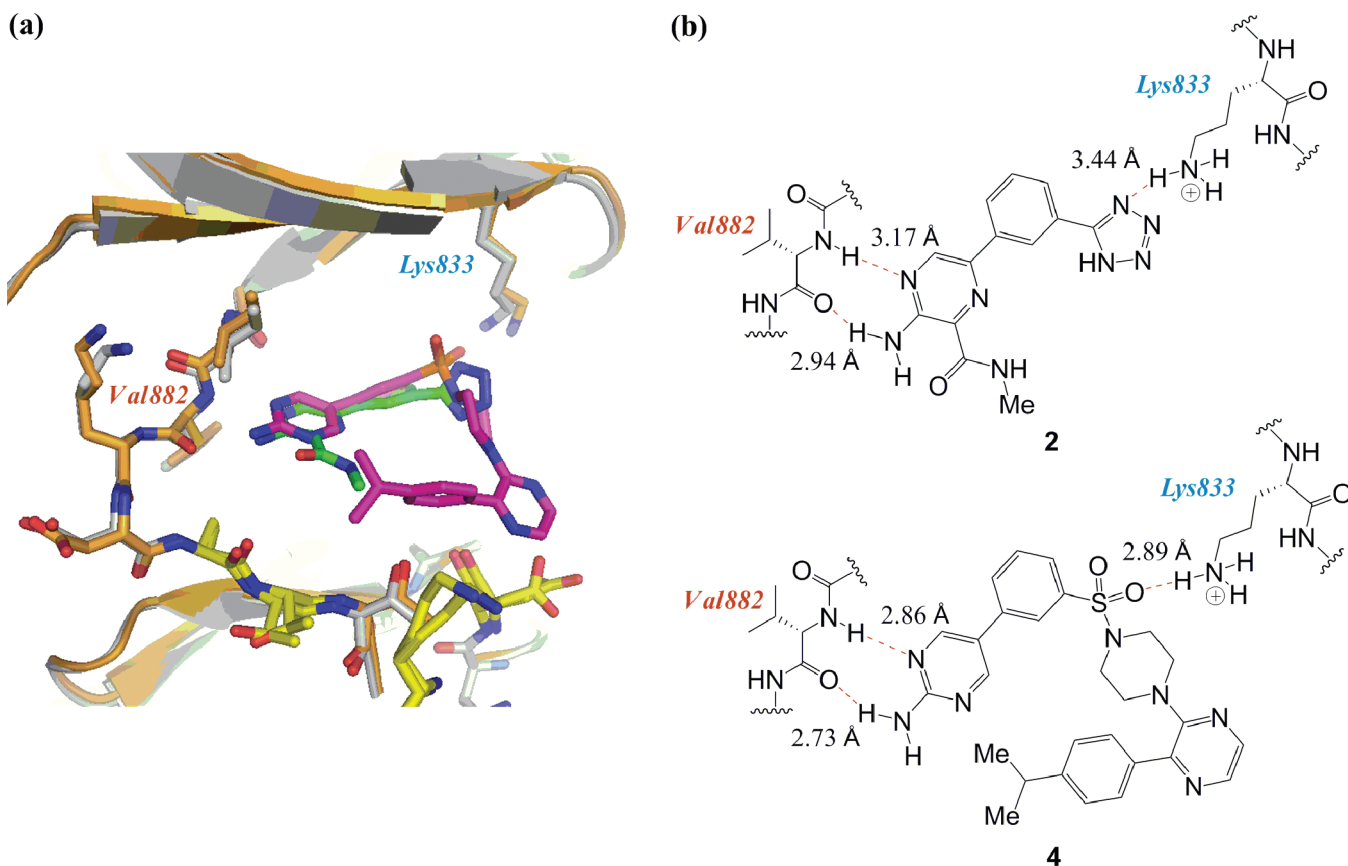


Figure 3. (a) Overlay of the cocrystal structures of 2/PI3K γ (green/gray) and 4/PI3K γ (magenta/orange). P-loop removed for clarity. Selectivity residues in close proximity to the ligands are displayed in yellow (PDB codes 4anu and 4anx). (b) Schematic presentation of the binding interactions between 2 and 4 in the active site.

replacement. Installation of a chlorine on the central ring generally led to an increase in cell activity as indicated with 8. This finding was further explored with reduction of the size of the sulfonamide group as demonstrated with 9–11 (Table 3). These analogues

Table 3. In Vitro Potency and Selectivity Data for Sulfonamide Derivatives of HTS Hit 2

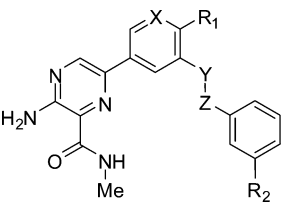
compd	R	PI3K γ IC ₅₀ (nM)	PI3K selectivity IC ₅₀ (nM)		
			α	β	δ
9	Me	17	142	1563	1073
10	H	26	97	701	638
11	CH ₂ CF ₃	65	752	2511	1418

were biochemically potent and provided evidence that the PI3K selectivity could be modulated by changing the alkyl group on the sulfonamide. Although the potency and selectivity was less than optimal with 11, it displayed acceptable oral plasma exposure in mice which provided affirmation of our thesis that a sulfonamide derivative with desirable solubility ($K_{\text{sol}} = 211 \mu\text{M}$) would improve the pharmacokinetic properties of this series.⁴⁹ We were particularly encouraged by the excellent cellular activity observed with aryl sulfonamide 8 and adopted it as a standard going forward.

Further derivatization involved modification of the scaffold core (Table 4). Comparison of methoxy analogue 12 with 8 and 13 suggested that electron withdrawing substituents improved the potency. Aminopyridine analogue 14 displayed a biochemical profile similar to that of parent 8, and reverse sulfonamide derivatives 15–16 displayed slightly decreased PI3K activity compared to that of parent 7. However, reintroduction of chlorine on the central ring increased the biochemical potency but decreased the selectivity profile as shown with a comparison of 16 and 17. Overall, alteration to the central ring of the aryl sulfonamide series did not lead to an improvement in the biochemical activity or selectivity profile.

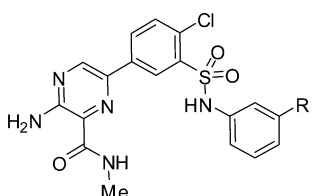
Building upon lead 8, substituted aryl sulfonamide derivatives were next considered. Changing substituents at the meta position, with groups exhibiting different electronic and steric properties, generally did not greatly alter the selectivity profile, cellular activity, or mouse plasma exposure as indicated by 18–22 (Table 5). However, walking a chlorine atom around the aryl group revealed that ortho substitution provided two significant advantages (22–24, Table 6). First, a >40-fold increase in plasma exposure in mice was observed for the ortho-substituted analogue 23 when compared to the meta-substituted analogue 22. Examination of the in vitro data for these analogues indicated that the explanation for the drastic difference in plasma exposure was likely related, at least in part, to differences in the solubility of 22 ($K_{\text{sol}} < 1 \mu\text{M}$) and 23 ($K_{\text{sol}} = 24 \mu\text{M}$). Second, ortho substitution incrementally improved the PI3K γ selectivity over other class I PI3Ks. As an aside, the slight potency improvement realized by placing a

Table 4. Biochemical Activity and PI3K Selectivity Data for Core Modifications of the Aryl Sulfonamide Series



compd	R ₁	X	Y	Z	R ₂	PI3K γ IC ₅₀ (nM)	PI3K selectivity IC ₅₀ (nM)		
							α	β	δ
12	OMe	C	SO ₂	NH	H	507	1807	>10,000	1202
13	F	C	SO ₂	NH	H	152	953	3370	1582
14	NH ₂	N	SO ₂	NH	H	53	200	362	533
15	H	C	NH	SO ₂	H	167	3643	>10,000	3389
16	H	C	NH	SO ₂	Cl	161	3381	6343	2964
17	Cl	C	NH	SO ₂	Cl	11	90	64	100

Table 5. PI3K Selectivity, Cellular Inhibition, and Mouse Plasma Exposure Data for meta-Substituted Aryl Sulfonamide Derivatives



compd	R	PI3K γ IC ₅₀ (nM)	PI3K γ cell IC ₅₀ (nM)	PI3K selectivity IC ₅₀ (nM)			mouse plasma exposure ^{a,b}
				α	β	δ	
18	Me	48	572	323	2075	568	n.d.
19	F	43	171	316	1611	415	1.6 ± 0.3 μ M (1 h) ^c 1.0 ± 0.1 μ M (4 h) ^c
20	OMe	31	431	290	1656	546	0.7 ± μ M (1 h) ^c 0.09 ± μ M (4 h) ^c
21	CF ₃	49	552	727	5070	1355	1.7 ± 0.7 μ M (1 h) ^d 0.4 ± 0.2 μ M (4 h) ^d
22	Cl	18	184	174	1130	437	1.3 ± 0.6 μ M (1 h) ^e 0.1 ± 0.04 μ M (4 h) ^e

^aData are reported as the mean \pm SD. ^bn.d. = not determined. ^cMale C57BL6 mice ($n = 3$) dosed at 100 mpk (PO) as a suspension in 10% EtOH 40% PEG400/water + 1:1 HCl. ^dFemale C57BL6 mice ($n = 3$) dosed at 100 mpk (PO) as a suspension in 0.75% CMC 0.1% Tween80/water. ^eMale C57BL6 mice ($n = 3$) dosed at 100 mpk (PO) as a suspension in 10% EtOH 60% PEG400/water.

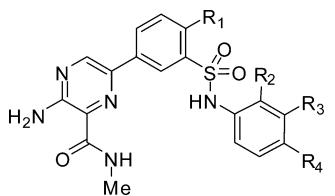
chlorine on the central ring with earlier analogues was also observed with a comparison of **22** and **25**.

In an effort to explore the scope of the encouraging data surrounding **23**, disubstituted aryl derivatives were pursued. Both **26** and **27** exhibited a profile similar to that of the parent **23** (Table 7). All other bis-substituted derivatives (**28–29** and **31–32**) also displayed excellent mouse plasma exposure. When comparing the high oral plasma exposure levels observed in mice for these analogues, in addition to solubility, permeability was a differentiating factor. Throughout the evolution of the program, passive membrane permeability was modeled using an MDCK cell-based assay, and the aryl sulfonamide series generally displayed apparent permeability (P_{app}) values of 100–200 nm/s. Therefore, it was not surprising to observe that **31** with excellent solubility ($K_{sol} = 176 \mu\text{M}$) and permeability (550 nm/s) displayed the highest oral plasma exposure in the bis-substituted aryl series. Additionally, a comparison of **30** and **31** again verified the potency increase observed when chlorine was placed on the central ring. Further SAR plans involved

optimization of the hinge-binding heterocycle utilizing the difluoroaryl sulfonamide contained in **31**.

An intriguing observation was made when considering the binding modes of **31** and **4** (Figure 4). As mentioned previously, the isopropyl group of **4** resides in a region containing multiple selectivity residues and was thought to contribute to the PI3K γ selectivity observed with this analogue. Therefore, a series of derivatives was synthesized to determine the extent to which the *N*-methylcarboxamide of **31** contributes to the PI3K selectivity profile since this group is in close proximity to the isopropyl group of **4** (Table 8). Analogue **33**, lacking the *N*-methylcarboxamide, displayed a significantly less attractive biochemical profile than **31**. However, the aminopyrimidine analogue **34** exhibited a biochemical profile similar to that of **31**, thereby providing evidence that the *N*-methylcarboxamide was not necessary to retain γ selectivity. Substitution at the 4-position of the pyrimidine to provide **35** and **36** incrementally increased the activity and deteriorated the PI3K selectivity. While it was intriguing that removal of the *N*-methylcarboxamide did not

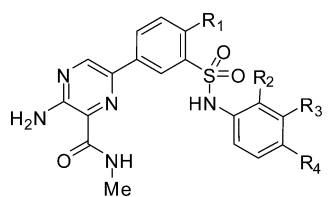
Table 6. PI3K Selectivity, Cellular Inhibition, and Mouse Plasma Exposure Data for Chloroaryl Sulfonamide Derivatives



compd	R ₁	R ₂	R ₃	R ₄	PI3K γ IC ₅₀ (nM)	PI3K γ cell IC ₅₀ (nM)	PI3K selectivity IC ₅₀ (nM)			mouse plasma exposure ^{a,b}
							α	β	δ	
23	Cl	Cl	H	H	20	507	476	2404	1020	59.1 ± 4.0 μ M (1 h) ^c 9.6 μ M ± 1.2(4 h) ^c
22	Cl	H	Cl	H	18	184	174	1130	437	1.3 ± 0.6 μ M (1 h) ^d 0.1 ± 0.04 μ M (4 h) ^d
24	Cl	H	H	Cl	26	394	142	1263	539	n.d.
25	H	H	Cl	H	42	409	705	4774	1253	0.6 ± 0.07 μ M (1 h) ^e 0.4 ± 0.1 μ M (4 h) ^e

^aData are reported as the mean ± SD. ^bn.d. = not determined. ^cMale C57BL6 mice ($n = 3$) dosed at 100 mpk (PO) as a suspension in 5% EtOH 40% PEG400/water. ^dMale BALB/c mice ($n = 3$) dosed at 100 mpk (PO) as a suspension in 10% EtOH 60% PEG400/water. ^eMale C57BL6 mice ($n = 3$) dosed at 100 mpk (PO) as a suspension in 0.75% CMC 0.1% Tween80/water.

Table 7. PI3K Selectivity, Cellular Inhibition, and Mouse Plasma Exposure Data for Bis-Substituted Aryl Sulfonamide Derivatives



compd	R ₁	R ₂	R ₃	R ₄	PI3K γ IC ₅₀ (nM)	PI3K γ cell IC ₅₀ (nM)	PI3K selectivity IC ₅₀ (nM)			mouse plasma exposure ^{a,b}
							α	β	δ	
26	Cl	Cl	H	F	5	528	209	1069	340	64.8 ± 7.1 μ M (1 h) ^c 19.2 ± 2.1 μ M (4 h) ^c
27	Cl	Cl	F	H	21	1575	972	4442	1186	236.7 ± 6.5 μ M (1 h) ^c 39.8 ± 6.5 μ M (4 h) ^c
28	Cl	Cl	H	Cl	8	464	323	1964	1032	21.3 ± 1.7 μ M (1 h) ^d 8.6 μ M ± 2.5 (4 h) ^d
29	Cl	Cl	Cl	H	18	587	555	1968	743	172.9 ± 32.3 μ M (1 h) ^d 22.1 ± 11.1 μ M (4 h) ^d
30	H	F	F	H	102	1877	2369	5016	2452	n.d.
31	Cl	F	F	H	18	773	435	2059	690	333.4 ± 8.3 μ M (1 h) ^e 119.3 μ M ± 40.6 (4 h) ^e
32	Cl	Me	F	H	34	805	342	1148	415	13.1 ± 4.1 μ M (1 h) ^e 6.2 ± 2.1 μ M (4 h) ^e

^aData are reported as the mean ± SD. ^bn.d. = not determined. ^cMale C57BL6 mice ($n = 3$) dosed at 100 mpk (PO) as a suspension in 0.75% CMC 0.1% Tween80/water. ^dMale C57BL6 mice ($n = 3$) dosed at 100 mpk (PO) as a suspension in 10% EtOH 20% PEG400/water. ^eMale C57BL6 mice ($n = 3$) dosed at 100 mpk (PO) as a suspension in 10% EtOH 40% PEG400/water + 1:1 HCl.

significantly influence γ selectivity, the inability to improve upon the biochemical profile of **31** prompted the deprioritization of effort in this area.

Select advanced analogues (**26**, **28**, and **31–32**) demonstrating >10-fold selectivity vs other PI3K class I isoforms, potent cellular activity, and excellent mouse plasma exposure were next examined in a pharmacodynamic assay (Table 9). Both genetic and pharmacological inhibitions of PI3K γ are known to reduce adenosine-evoked mast cell degranulation in vivo.^{16,50} To determine the ability of our advanced PI3K γ inhibitors to affect mast cell activation in an inflammatory response, they were tested in an established adenosine-induced mast cell

degranulation (AIMCD) mouse in vivo model. Response was measured by quantitating Evans' blue dye extravasation at 4 h in the ears of BALB/c mice. Of note, **26**, **28**, **31**, and **32** exhibit a response analogous to that observed with PI3K γ -deficient mice in this assay.⁵⁰ Additionally, data for **37** (GDC-0941),⁵¹ a well characterized pan-active PI3K inhibitor currently in clinical trials, provided evidence that knock-down in this assay was not enhanced by additional inhibition of other PI3K isoforms. A comparison of **32** to the potent anti-inflammatory steroid dexamethasone, indicated that while **32** was less potent, it induced a significant degranulation response in this assay (Figure 5).

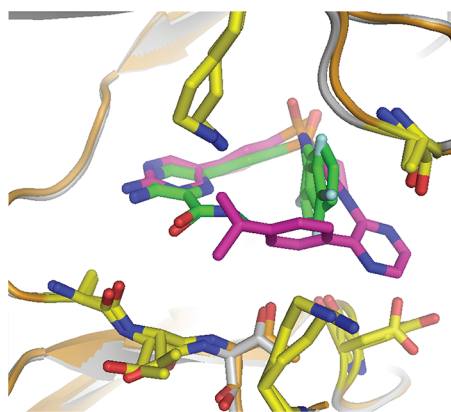


Figure 4. Overlay of cocrystal structures of **31**/PI3K γ (green/gray) and **4**/PI3K γ (magenta/orange) with selectivity residues displayed in yellow (PDB codes 4anu and 4anw). The difluorophenyl ring of **31** was found to be present and modeled in two equivalently populated poses, related by a 180° flip of the ring plane.

Table 8. Hinge-Binding Heterocycle Derivatives of **31**

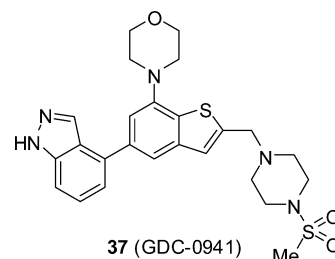
compd	R	PI3K γ IC ₅₀ (nM)	PI3K selectivity IC ₅₀ (nM)		
			α	β	δ
33		497	4647	6275	4389
34		60	1663	2643	1316
35		20	234	54	181
36		6	110	39	41

Given the established link between PI3K γ in preventing joint damage and neutrophil recruitment in mouse models of rheumatoid arthritis,⁴³ an experiment was undertaken to measure the impact that **32** would have on neutrophil migration (Figure 6). In mice, intraperitoneal injection of the chemokine RANTES (CCL5) is known to induce neutrophil recruitment to the peritoneal cavity.⁴³ Oral administration of **32** resulted in a 50% reduction in neutrophil recruitment, thereby providing evidence of the effect PI3K γ inhibition can exhibit on neutrophil migration in vivo.

On the basis of the desirable profile of **31** and **32** in the mouse, full pharmacokinetic data was gathered in rat (Table 10). Generally, the exposure data observed between the mouse and rat correlated appropriately where **31** demonstrated significantly higher plasma levels than **32** in both species. High plasma exposure levels were observed for both analogues administered as a solution. Bioavailabilities were >60% at 5 mpk along with a half-life of >4 h for **31**. Figure 7 shows the pharmacokinetic profile of **31** when dosed as a solution in the rat at 5 mpk.

Additionally, advanced leads **31** and **32** were also profiled against a set of kinase targets using previously described methods (Table 11).^{52,53} The IC₅₀ inhibition measured for

Table 9. In Vivo Data for Aryl Sulfonamide Advanced Leads and Pan-Active PI3K Inhibitor **37**



compd	PI3K γ IC ₅₀ (nM)	PI3K γ cell IC ₅₀ (nM)	adenosine induced mast cell degranulation (%) ^a	mouse plasma exposure (4 h) ^b
26	5	528	61 ± 25	20.3 ± 5.8 μ M ^c
28	8	464	65 ± 15	6.5 ± 1.1 μ M ^d
31	18	773	63 ± 21	43.1 ± 7.9 μ M ^e
32	34	805	72 ± 12	9.2 ± 3.1 μ M ^c
37	42	298	29 ± 19	5.3 ± 2.1 μ M ^e

^aResponse was measured by quantitating Evans' blue (% absorbance at 620 nm relative to vehicle, mean ± SD, $n \geq 8$) extravasation at 4 h in the ears of male BALB/c mice. Analogues were dosed at 100 mpk orally. ^bData are reported as the mean ± SD. ^cMale BALB/c mice ($n \geq 8$) dosed at 100 mpk (PO) as a suspension in 10% EtOH 40% PEG400/water + 1:1 HCl. ^dMale BALB/c mice ($n = 8$) dosed at 100 mpk (PO) as a suspension in 10% EtOH 40% PEG400/water. ^eMale BALB/c mice ($n = 10$) dosed at 100 mpk (PO) as a suspension in 0.5% CMC 0.2% Tween80/water.

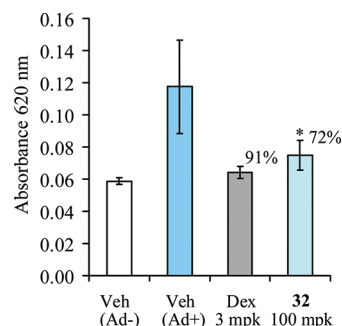


Figure 5. Inhibition of adenosine-induced mast cell degranulation (AIMCD) by **32** dosed orally at 100 mpk. Response was measured by quantitating Evans' blue extravasation in the ears of male BALB/c mice at 4 h. Data are reported as the mean ± SD ($n = 8$, $*P < 0.05$). Vehicle (Ad-, nonsensitized) and Vehicle (Ad+, adenosine sensitized) formulation: 10% EtOH 40% PEG400/water + 1:1 HCl. Dexamethasone (Dex) dosed PO at 3 mpk in 0.5% CMC/0.2% Tween80. Analogue **32** was dosed as a suspension in 10% EtOH 40% PEG400/water + 1:1 HCl.

31 and **32** against the vast majority of kinases tested was >3600 nM. Not surprisingly, cross-reactivity with the closely related kinase mTOR was observed in both analogues.⁵⁴ The CYP, hERG, and P-glycoprotein inhibition profile of **31** was also characterized (Table 12). The IC₅₀ inhibition measured was >20,000 nM with the majority of ADME targets profiled. Collectively, the attractive off-target selectivity and ADME profile of **31** will allow this analogue to serve as a useful pharmacological tool.

Chemistry. Outlined in Scheme 1 is the synthesis of HTS hit **1**. Deprotection of **38** under acidic conditions followed by coupling with 3-bromobenzene-1-sulfonyl chloride provided bromide **39**. A Suzuki–Miyaura cross-coupling utilizing two

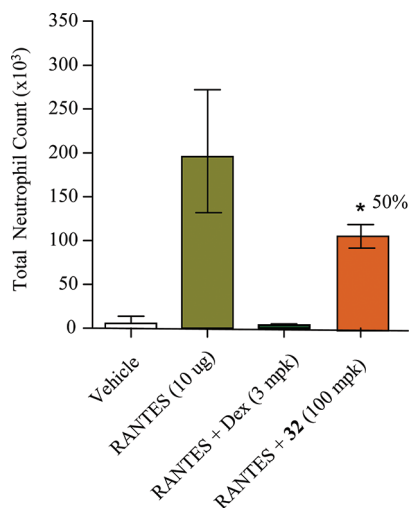


Figure 6. Analogue **32** dosed orally in male BALB/c mice at 100 mpk reduced RANTES-induced peritoneal neutrophil recruitment in vivo by 50%. Total neutrophil count was quantitated using FACS analysis. Data are reported as the mean \pm SD ($n = 5$, $*P = <0.05$). Vehicle formulation: 10% EtOH 40% PEG400/water + 1:1 HCl. Dexamethasone (Dex) dosed PO at 3 mpk in 0.5% CMC/0.2% Tween80. Analogue **32** was dosed as a suspension in 10% EtOH 40% PEG400/water + 1:1 HCl.

Table 10. Oral Pharmacokinetic Parameters for **31** and **32** in Rat (5 mpk, PO)^a

compd	C_{max} (μM)	parameter		
		$t_{1/2}$ (h)	AUC _(0-∞) ($\mu M \cdot h$)	% F
31	42.5	4.44	449.4	76.7
32	9.1	2.08	26.77	66.2

^aAnalogues were dosed in female Sprague–Dawley rats ($n = 3$) as a solution in 10% NMP 60% PEG400/water.

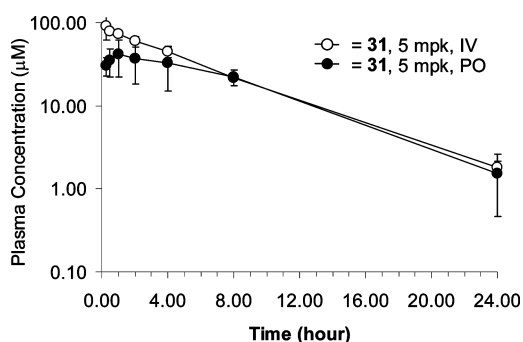


Figure 7. Pharmacokinetic profile of **31** in rat. Dosed as a solution in female Sprague–Dawley rats at 5 mpk using IV formulation, 10% NMP 60% PEG400/water + 1:1 HCl, and PO formulation, 10% NMP 60% PEG400/water. Data are reported as the mean \pm SD ($n = 3$).

equivalents of 4-methoxyphenylboronic acid provided the final product **1**.

The synthesis of **3** was carried out in 3 steps starting from intermediate **39** (Scheme 2). First, a Suzuki–Miyaura cross-coupling with one equivalent 4-methoxyphenylboronic acid provided **40**, which was followed by boronic ester formation and another Suzuki–Miyaura coupling with 5-bromopyrimidin-2-amine.

Analogue **4** was constructed as outlined in Scheme 3. The 3-bromobenzene-1-sulfonyl chloride was first coupled to

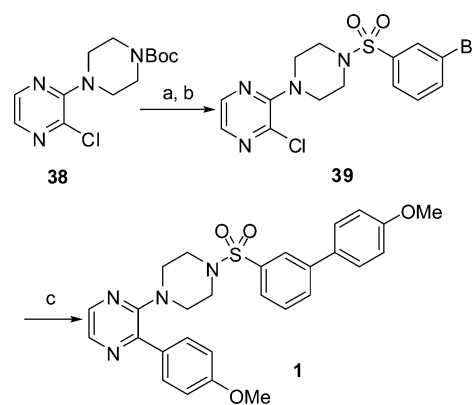
Table 11. Kinase Selectivity Profile of **31** and **32**

kinase	31 inhibition IC ₅₀ (nM)	32 inhibition IC ₅₀ (nM)
AKT1	>3600	>3600
Aurora B	>3600	>3600
c-Met	>3600	>3600
cdc7 MP	>3600	>3600
cdk1-cyclinB	>3600	>3600
Chk1 MP	>3600	>3600
cRaf-1	206	1814
cRAF/MEK1/ERK2	2313	2043
EGFR	739	410
FGFR1	>3600	>3600
Flt-3	>3600	>3600
hPKA Kem	>3600	>3600
IRK	>3600	>3600
JAK2	>3600	>3600
KDR	>3600	>3600
p70S6k	>3600	>3600
PDGFRB	>3600	>3600
PDK1	>3600	>3600
PKCbetaII	>3600	>3600
SRC MP	>3600	>3600
mTOR/GbL/Raptor	623	1781

Table 12. CYP450, hERG, and P-gp Inhibition Profile of Compound **31**

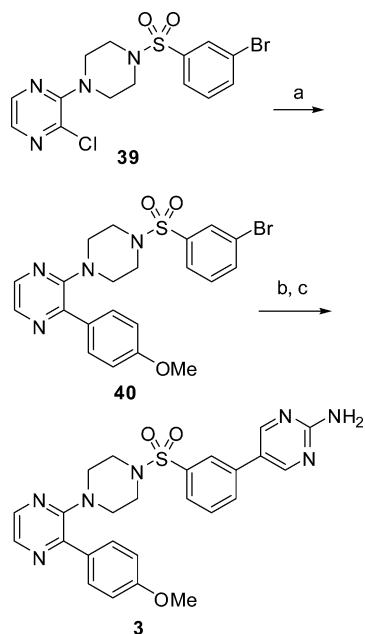
target	inhibition IC ₅₀ (nM)
CYP1A2	>20,000
CYP2C19	>20,000
CYP2C8	2331
CYP2C9	591
CYP2D6*1	>20,000
CYP3A4 (substrate: midazolam)	>20,000
CYP3A4 (substrate: testosterone)	>20,000
hERG potassium channel	17,318
P-glycoprotein	>20,000

Scheme 1^a



^aReagents: (a) 4 N HCl, 1,4-dioxane, rt; (b) *N,N*-diisopropylethylamine, CH₂Cl₂, 3-bromobenzene-1-sulfonyl chloride, 0 °C; (c) 4-methoxyphenylboronic acid, Pd(dppf)Cl₂·CH₂Cl₂, potassium carbonate, 1,4-dioxane, H₂O, 90 °C.

tert-butyl piperazine-1-carboxylate to provide **41**, followed by a Miyaura borylation and Suzuki–Miyaura cross-coupling with 5-bromopyrimidin-2-amine to provide **42**. Deprotection under

Scheme 2^a

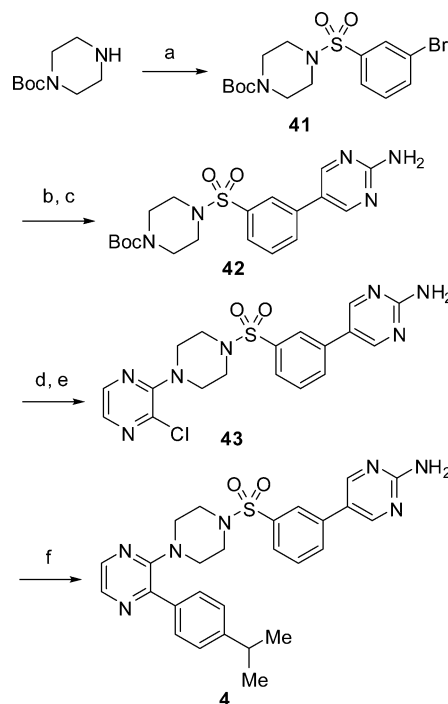
^aReagents: (a) 4-methoxyphenylboronic acid, tetrakis(triphenylphosphine)palladium(0), potassium carbonate, 1,4-dioxane, H₂O 70 °C; (b) bis(pinacolato)diboron, Pd(dppf)Cl₂·CH₂Cl₂, potassium acetate, 1,2-dimethoxyethane, 90 °C; (c) 5-bromopyrimidin-2-amine, Pd(dppf)Cl₂·CH₂Cl₂, potassium carbonate, 1,4-dioxane, H₂O, 90 °C.

acidic conditions followed by coupling with 2,3-dichloropyrazine afforded **43**, and a Suzuki–Miyaura cross-coupling with 4-isopropylphenylboronic acid provided the final product **4**.

The synthesis of optimized lead **5** is described in Scheme 4. A Buchwald–Hartwig cross-coupling was used to fuse 3-bromo-2-chloropyridine to *tert*-butyl piperazine-1-carboxylate followed by a Suzuki–Miyaura cross-coupling to provide **44**. Deprotection under acidic conditions followed by coupling with 3-bromobenzene-1-sulfonyl chloride provided **45**. Lastly, the Miyaura borylation/Suzuki–Miyaura cross-coupling sequence used to synthesize **4** was also proficient in providing **5**.

The synthesis of 3-aminopyrazine-2-carboxamides **7–13** and **18–32** is outlined in Scheme 5. Analogue **14** was synthesized using a procedure similar to that outlined in Scheme 5 starting from the known 2-amino-5-bromopyridine-3-sulfonyl chloride.⁵⁵ The noncommercially available sulfonyl chlorides were obtained via a modified Sandmeyer reaction and subsequently coupled to the appropriate amine.⁵⁶ The sulfonamide substrate was then subjected to a single-flask two-step sequence involving a Miyaura borylation reaction followed by a Suzuki–Miyaura cross-coupling reaction with 3-amino-6-bromo-*N*-methylpyrazine-2-carboxamide to yield the corresponding analogue.

The synthesis of reverse sulfonamide derivatives **15–17** outlined in Scheme 6 was carried out by coupling the appropriate aniline to the corresponding aryl sulfonyl chloride. In a similar fashion to the analogues synthesized in Scheme 2, a Suzuki–Miyaura cross-coupling was utilized to provide the final compounds. Likewise, the aminopyrimidine derivatives **33–36** shown in Scheme 7 were also synthesized in a manner similar to that used for the derivatives in Scheme 2 but substituting the appropriate aminopyrimidine in place of 3-amino-6-bromo-*N*-methylpyrazine-2-carboxamide.

Scheme 3^a

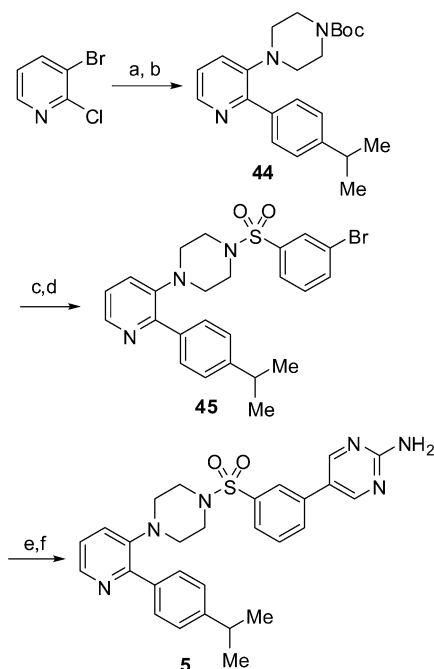
^aReagents: (a) *N,N*-diisopropylethylamine, CH₂Cl₂, 3-bromobenzene-1-sulfonyl chloride, 0 °C; (b) bis(pinacolato)diboron, Pd(dppf)Cl₂·CH₂Cl₂, potassium acetate, 1,2-dimethoxyethane, 90 °C; (c) 5-bromopyrimidin-2-amine, tetrakis(triphenylphosphine)palladium(0), potassium carbonate, 1,4-dioxane, H₂O, 90 °C; (d) 4 N HCl, 1,4-dioxane, rt; (e) 2,3-dichloropyrazine, potassium carbonate, dimethylacetamide, 120 °C; (f) 4-isopropylphenylboronic acid, Pd(dppf)Cl₂·CH₂Cl₂, potassium carbonate, 1,4-dioxane, H₂O, 90 °C.

CONCLUSIONS

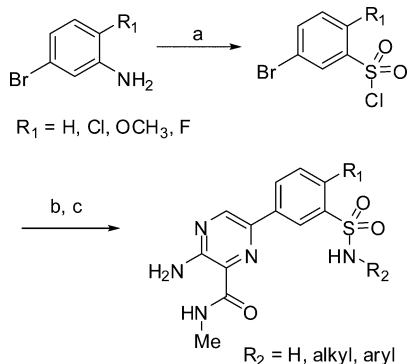
A series of novel, highly potent, and selective PI3K γ inhibitors are disclosed. The sulfonylpiperazine series was optimized utilizing structure-based design; however, despite improving the potency and selectivity of this series, desirable pharmacokinetic properties could not be achieved. Taking advantage of insight from cocrystal structures of **4** and HTS hit **2** in PI3K γ provided a series of novel hybrid sulfonamide analogues with improved physical properties and pharmacokinetics. Pharmacodynamic data for lead analogues provided a response similar to that observed for PI3K γ deficient mice. In summary, advanced leads such as **31** contain a desirable potency, selectivity, and pharmacokinetic profile that will contribute both biological and chemical insights into the developing area of PI3K research for the study of inflammatory disease.

EXPERIMENTAL SECTION

All reagents and solvents employed were purchased commercially and used without further purification unless otherwise indicated. NMR spectra were recorded on a Varian Mercury Plus 400 MHz instrument. Reported spectra may appear to contain superfluous signals due to the existence of rotamers and/or carbon–fluorine coupling. Chemical shifts are reported in parts per million (ppm) relative to an internal standard of tetramethylsilane in deuterated dimethyl sulfoxide (DMSO-*d*₆), deuterated methanol (CD₃OD), or deuterated chloroform (CDCl₃). All final compounds were purified to $\geq 95\%$ purity as assayed by analytical HPLC (YMC-Pack Pro 150 \times 4.6 mm, 5 μ m C18 column, Shimadzu LC-10AT VP system equipped with a Shimadzu SPD-M10A VP diode array detector) at a 1.5 mL/min flow rate with a

Scheme 4^a

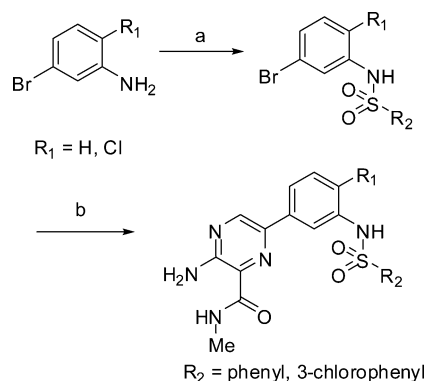
^aReagents: (a) *tert*-butyl piperazine-1-carboxylate, xantphos, tris(dibenzylideneacetone)dipalladium(0), sodium *tert*-butoxide, toluene, 100 °C; (b) 4-isopropylphenylboronic acid, Pd(dppf)Cl₂·CH₂Cl₂, potassium carbonate, 1,4-dioxane, H₂O, 90 °C; (c) 4 N HCl, 1,4-dioxane, rt; (d) *N,N*-diisopropylethylamine, CH₂Cl₂, 3-bromobenzene-1-sulfonyl chloride, rt; (e) bis(pinacolato)diboron, Pd(dppf)Cl₂·CH₂Cl₂, potassium acetate, 1,2-dimethoxyethane, 90 °C; (f) 5-bromopyrimidin-2-amine, Pd(dppf)Cl₂·CH₂Cl₂, potassium carbonate, 1,4-dioxane, H₂O, 90 °C.

Scheme 5^a

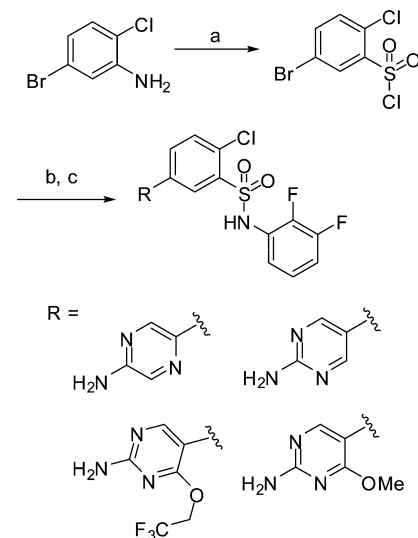
^aReagents: (a) NaNO₂, H₂O, HCl, 0 °C; SO₂, CuCl, AcOH, 0 °C to rt; (b) R₂NH₂, pyridine, CH₂Cl₂, rt; (c) bis(pinacolato)diboron, Pd(dppf)Cl₂·CH₂Cl₂, potassium acetate, dioxane, 90 °C; 3-amino-6-bromo-*N*-methylpyrazine-2-carboxamide, triethylamine, Pd(dppf)Cl₂·CH₂Cl₂, triethylamine, *N,N*-dimethylformamide, H₂O, 85 °C.

gradient of 5–95% acetonitrile (containing 0.1% TFA) in 0.1% aqueous TFA for 25 min and total run time of 27 min. Analogues **2** and **6** were synthesized as previously described.⁴⁵ Mouse liver microsomes assay data, reported as the mean ± SD, was carried out as previously described.⁵⁷

2-(4-(4'-Methoxybiphenyl-3-ylsulfonyl)piperazin-1-yl)-3-(4-methoxyphenyl)pyrazine (1). To a stirred solution of **38** (896 mg, 3.00 mmol) in 1,4-dioxane (20 mL) was added HCl (5 mL, 4 N in 1,4-dioxane), and the reaction mixture was stirred at ambient temperature

Scheme 6^a

^aReagents: (a) 3-bromoaniline or 5-bromo-2-chloroaniline, pyridine, CH₂Cl₂, rt; (b) bis(pinacolato)diboron, Pd(dppf)Cl₂·CH₂Cl₂, potassium acetate, dioxane, 90 °C; 3-amino-6-bromo-*N*-methylpyrazine-2-carboxamide, triethylamine, Pd(dppf)Cl₂·CH₂Cl₂, triethylamine, *N,N*-dimethylformamide, H₂O, 85 °C.

Scheme 7^a

^aReagents: (a) NaNO₂, H₂O, HCl, 0 °C; SO₂, CuCl, AcOH, 0 °C to rt; (b) 2,3-difluoroaniline, pyridine, CH₂Cl₂, rt; (c) bis(pinacolato)diboron, Pd(dppf)Cl₂·CH₂Cl₂, potassium acetate, dioxane, 90 °C; RBr, Pd(dppf)Cl₂·CH₂Cl₂, triethylamine, *N,N*-dimethylformamide, H₂O, 85 °C.

for 2 h. The reaction mixture was concentrated and used directly for the next step.

To a stirred mixture of crude piperazine (962 mg, 3.00 mmol), *N,N*-diisopropylethylamine (2.61 mL, 15.0 mmol), and CH₂Cl₂ (20 mL) was added 3-bromobenzene-sulfonyl chloride (770 mg, 3.03 mmol) dropwise at 0 °C. After stirring for 30 min, saturated sodium bicarbonate was added, and the resulting solution was extracted with CH₂Cl₂ (2×). The combined organic layers were dried over anhydrous sodium sulfate and concentrated, and the residue was triturated with ethyl acetate and hexanes to afford **39** (1.04 g, 83%).

A mixture of **39** (125 mg, 0.300 mmol), 4-methoxyphenylboronic acid (137 mg, 0.901 mmol), potassium carbonate (415 mg, 3.00 mmol), Pd(dppf)Cl₂·CH₂Cl₂ (49.0 mg, 60.0 μmol), 1,4-dioxane (4 mL), and H₂O (1 mL) was stirred at 90 °C for 2 h. The reaction mixture was concentrated and purified by flash chromatography (hexanes/ethyl acetate, 2:1) to provide **1** (117 mg, 75%) as a white powder after lyophilization. ¹H NMR (400 MHz, CDCl₃) δ 8.14 (d, *J* = 2.5 Hz, 1H), 8.01 (d, *J* = 2.5 Hz, 1H), 7.91 (t, *J* = 1.7 Hz, 1H),

7.84–7.79 (m, 1H), 7.77–7.72 (m, 2H), 7.70–7.66 (m, 1H), 7.61 (d, $J = 7.7$ Hz, 1H), 7.59–7.54 (m, 2H), 7.05–7.01 (m, 2H), 6.89–6.84 (m, 2H), 3.88 (s, 3H), 3.80 (s, 3H), 3.32–3.22 (m, 4H), 3.12–3.00 (m, 4H). MS (EI) for $C_{28}H_{28}N_4O_4S$, found 517.2 (MH⁺).

5-(3-(4-(3-(4-Methoxyphenyl)pyrazin-2-yl)piperazin-1-ylsulfonyl)phenyl)pyrimidin-2-amine (3). A mixture of **39** (251 mg, 0.603 mmol), 4-methoxyphenylboronic acid (91.0 mg, 0.599 mmol), potassium carbonate (415 mg, 3.00 mmol), tetrakis(triphenylphosphine)palladium(0) (69.4 mg, 60.0 μ mol), 1,4-dioxane (4 mL), and H₂O (1 mL) was stirred at 70 °C for 2 h. The reaction mixture was concentrated and purified by flash chromatography (hexanes/ethyl acetate, 5:1) to provide **40** (251 mg, 85%).

A mixture of **40** (251 mg, 0.510 mmol), bis(pinacolato)diboron (260 mg, 1.02 mmol), Pd(dppf)Cl₂·CH₂Cl₂ (41.6 mg, 51.0 μ mol), potassium acetate (200 mg, 2.04 mmol), and 1,2-dimethoxyethane (6 mL) was stirred at 90 °C for 2 h. The reaction mixture was cooled to ambient temperature, concentrated, and purified by flash chromatography (hexanes/ethyl acetate, 3:1) followed by trituration with hexanes to afford 2-(4-methoxyphenyl)-3-(4-(3-(4,4,5,5-tetramethyl-1,3,2-dioxaborolan-2-yl)phenylsulfonyl)piperazin-1-yl)pyrazine (236 mg, 86%) as an off-white solid.

A mixture of 2-(4-methoxyphenyl)-3-(4-(3-(4,4,5,5-tetramethyl-1,3,2-dioxaborolan-2-yl)phenylsulfonyl)piperazin-1-yl)pyrazine (96.5 mg, 0.180 mmol), 5-bromopyrimidin-2-amine (41.5 mg, 0.240 mmol), potassium carbonate (150 mg, 1.09 mmol), Pd(dppf)Cl₂·CH₂Cl₂ (16.3 mg, 20 μ mol), 1,4-dioxane (4 mL), and H₂O (1 mL) was stirred at 90 °C for 1 h. The reaction mixture was cooled to ambient temperature, concentrated, and purified by flash chromatography (ethyl acetate/hexanes, 3:1) to afford **3** (54.0 mg, 60%) as a white powder after lyophilization. ¹H NMR (400 MHz, CDCl₃) δ 8.57 (s, 2H), 8.15 (d, $J = 2.0$ Hz, 1H), 8.02 (d, $J = 2.0$ Hz, 1H), 7.86 (br s, 1H), 7.76–7.73 (m, 4H), 7.65 (t, $J = 8.4$ Hz, 1H), 6.88 (d, $J = 8.4$ Hz, 2H), 5.29 (s, 2H), 3.83 (s, 3H), 3.30–3.28 (m, 4H), 3.10–3.08 (m, 4H). MS (EI) for $C_{25}H_{25}N_7O_3S$, found 504.1 (MH⁺).

5-(3-(4-(3-(4-Isopropylphenyl)pyrazin-2-yl)piperazin-1-ylsulfonyl)phenyl)pyrimidin-2-amine (4). To a stirred solution of *tert*-butyl piperazine-1-carboxylate (5.59 g, 30.0 mmol) and *N,N*-diisopropylethylamine (6.30 mL, 36.0 mmol) in CH₂Cl₂ (60 mL) was added 3-bromobenzene-1-sulfonyl chloride dropwise at 0 °C. After stirring for 30 min, H₂O was added, and the resulting solution was extracted with CH₂Cl₂ (2 \times). The combined organic layers were dried over anhydrous sodium sulfate, concentrated, and purified by flash chromatography (hexanes/ethyl acetate, 5:1) followed by trituration with hexanes to provide **41** (11.9 g, 98%) as an off-white solid.

A mixture of **41** (8.10 g, 20.0 mmol), bis(pinacolato)diboron (10.2 g, 40.0 mmol), Pd(dppf)Cl₂·CH₂Cl₂ (820 mg, 1.00 mmol), potassium acetate (7.85 g, 80.0 mmol), and 1,2-dimethoxyethane (40 mL) was stirred at 90 °C for 2 h. The reaction mixture was cooled to ambient temperature, concentrated, and purified by flash chromatography (hexanes/ethyl acetate, 5:1) followed by trituration with hexanes to afford *tert*-butyl 4-(3-(4,4,5,5-tetramethyl-1,3,2-dioxaborolan-2-yl)phenylsulfonyl)piperazine-1-carboxylate (9.1 g, quant.) as a pale pink solid.

A mixture of *tert*-butyl 4-(3-(4,4,5,5-tetramethyl-1,3,2-dioxaborolan-2-yl)phenylsulfonyl)piperazine-1-carboxylate (9.10 g, 20.0 mmol), 5-bromopyrimidin-2-amine (3.48 g, 20.0 mmol), potassium carbonate (8.30 g, 60.0 mmol), and tetrakis(triphenylphosphine)palladium(0) (817 mg, 1.00 mmol), 1,4-dioxane (40 mL), and H₂O (10 mL) was stirred at 90 °C for 1 h. The reaction mixture was cooled to ambient temperature, concentrated, and purified by flash chromatography (ethyl acetate/hexanes 3:1) followed by trituration with ethyl acetate to afford **42** (6.49 g, 77%) as an off-white solid.

To a stirred solution of **42** (6.49 g, 15.4 mmol) in 1,4-dioxane (60 mL) was added HCl (30 mL, 4 N in 1,4-dioxane), and the resulting mixture was stirred at ambient temperature overnight. The reaction mixture was concentrated and used for the next step without further purification.

A mixture of crude 5-(3-(piperazin-1-ylsulfonyl)phenyl)pyrimidin-2-amine, potassium carbonate (21.3 g, 154 mmol), 2,3-dichloropyrazine (3.44 g, 23.1 mmol) in dimethylacetamide (120 mL) was stirred

at 120 °C overnight. The reaction mixture was cooled to ambient temperature, diluted with H₂O, the precipitate was collected, and the separated aqueous layer was extracted with ethyl acetate (2 \times). The combined organic layers were dried over anhydrous sodium sulfate and concentrated to give a light-brown solid. The solid and precipitate were combined, triturated with ethyl acetate, filtered, and dried to afford **43** (4.5 g). Another crop (0.3 g) was precipitated from the filtrate to provide a total yield of 72% in this manner.

A mixture of **43** (43 mg, 99.5 μ mol), 4-isopropylphenylboronic acid (24.6 mg, 0.150 mmol), potassium carbonate (69.0 mg, 0.500 mmol), and Pd(dppf)Cl₂·CH₂Cl₂ (8.2 mg, 10 μ mol), 1,4-dioxane (4 mL), and H₂O (1 mL) was stirred at 90 °C for 1 h. The reaction mixture was cooled to ambient temperature, concentrated, and purified by flash chromatography (ethyl acetate/hexanes, 4:1) to afford **4** (32.0 mg, 62%) as a white powder after lyophilization. ¹H NMR (400 MHz, DMSO-*d*₆) δ 8.67 (s, 2H), 8.18 (d, $J = 2.5$ Hz, 1H), 8.11 (d, $J = 2.5$ Hz, 1H), 8.03 (d, $J = 7.9$ Hz, 1H), 7.87 (s, 1H), 7.77–7.62 (m, 4H), 7.19 (d, $J = 8.2$ Hz, 2H), 6.97 (s, 2H), 3.17–3.14 (m, 4H), 2.97–2.95 (m, 4H), 2.85 (dt, $J = 13.9, 7.1$ Hz, 1H), 1.17 (d, $J = 6.9$ Hz, 6H). MS (EI) for $C_{27}H_{29}N_7O_3S$, found 516.3 (MH⁺).

5-(3-(4-(2-(4-Isopropylphenyl)pyridin-3-yl)piperazin-1-ylsulfonyl)phenyl)pyrimidin-2-amine (5). A solution of 3-bromo-2-chloropyridine (750 mg, 3.90 mmol), *tert*-butyl piperazine-1-carboxylate (559 mg, 3.00 mmol), sodium *tert*-butoxide (432 mg, 4.50 mmol), tris(dibenzylideneacetone)dipalladium(0) (55.0 mg, 60.0 μ mol), xantphos (104 mg, 0.180 mmol), and toluene (15 mL) was stirred at 100 °C for 2 h. The reaction mixture was cooled to ambient temperature, diluted with H₂O, extracted with ethyl acetate (2 \times), and washed with brine. The separated organic layer was dried over sodium sulfate, concentrated, and purified by flash chromatography (hexanes/ethyl acetate, 10:1) to give *tert*-butyl 4-(2-chloropyridin-3-yl)piperazine-1-carboxylate (747 mg, 84%).

A mixture of *tert*-butyl 4-(2-chloropyridin-3-yl)piperazine-1-carboxylate (505 mg, 1.70 mmol), 4-isopropylphenylboronic acid (335 mg, 2.00 mmol), potassium carbonate (705 mg, 5.10 mmol), Pd(dppf)Cl₂·CH₂Cl₂ (139 mg, 0.170 mmol), 1,4-dioxane (15 mL), and H₂O (5 mL) was stirred at 90 °C for 1 h. The reaction mixture was cooled to ambient temperature, concentrated, and purified by flash chromatography (hexanes/ethyl acetate, 10:1) to afford **44** (541 mg, 84%).

To a stirred solution of **44** (541 mg, 1.42 mmol) in 1,4-dioxane (8 mL) was added HCl (5 mL, 4 N in 1,4-dioxane), and the reaction mixture was stirred at ambient temperature overnight. The reaction mixture was concentrated and used directly for the next step.

To a stirred mixture of crude 1-(2-(4-isopropylphenyl)pyridin-3-yl)piperazine and *N,N*-diisopropylethylamine (1.23 mL, 3.75 mmol) in CH₂Cl₂ (6 mL) was added 3-bromophenylsulfonyl chloride (397 mg, 1.55 mmol). After stirring for 30 min at ambient temperature, H₂O was added, and the resulting solution was extracted with CH₂Cl₂ (2 \times). The combined organic layers were dried over anhydrous sodium sulfate, concentrated, and purified by flash chromatography (hexanes/ethyl acetate, 3:1) to provide **45** (647 mg, 92% in 2 steps).

A mixture of **45** (375 mg, 0.750 mmol), bis(pinacolato)diboron (571 mg, 2.25 mmol), Pd(dppf)Cl₂·CH₂Cl₂ (61.2 mg, 75.0 μ mol), potassium acetate (442 mg, 4.50 mmol), and 1,2-dimethoxyethane (8 mL) was stirred at 90 °C for 1 h. The reaction mixture was cooled to ambient temperature, concentrated, and purified by flash chromatography (hexanes/ethyl acetate, 2:1) followed by trituration with hexanes to afford 1-(2-(4-isopropylphenyl)pyridin-3-yl)-4-(3-(4,4,5,5-tetramethyl-1,3,2-dioxaborolan-2-yl)phenylsulfonyl)piperazine (337 mg, 82%) as a white powder.

A mixture of 1-(2-(4-isopropylphenyl)pyridin-3-yl)-4-(3-(4,4,5,5-tetramethyl-1,3,2-dioxaborolan-2-yl)phenylsulfonyl)piperazine (137 mg, 0.250 mmol), 5-bromopyrimidin-2-amine (51.9 mg, 0.300 mmol), potassium carbonate (138 mg, 1.00 mmol), Pd(dppf)Cl₂·CH₂Cl₂ (20.4 mg, 25.0 μ mol), 1,4-dioxane (4 mL), and H₂O (1 mL) was stirred at 90 °C for 1 h. The reaction mixture was cooled to ambient temperature, concentrated, and purified by flash chromatography (ethyl acetate/hexanes, 3:1) followed by reverse phase HPLC (acetonitrile/aqueous ammonium acetate buffer solution; 30–100% gradient) to provide **5** (64.0 mg, 50%) as a white powder after

lyophilization. ^1H NMR (400 MHz, DMSO- d_6) δ 8.69 (s, 2H), 8.27 (dd, $J = 4.0, 1.2$ Hz, 1H), 8.07 (t, $J = 1.2$ Hz, 1H), 7.87 (t, $J = 1.6$ Hz, 1H), 7.75 (t, $J = 8.0$ Hz, 1H), 7.67–7.65 (m, 3H), 7.47 (dd, $J = 8.4, 1.6$ Hz, 1H), 7.26 (dd, $J = 8.4, 4.8$ Hz, 1H), 7.06 (d, $J = 8.4$ Hz, 2H), 6.98 (s, 2H), 2.91–2.74 (m, 9H), 1.11 (d, $J = 7.2$ Hz, 6H). MS (EI) for $\text{C}_{28}\text{H}_{30}\text{N}_6\text{O}_3\text{S}$ found 515.1 (MH $^+$).

3-Amino-6-(4-chloro-3-(*N*-*m*-tolylsulfamoyl)phenyl)-*N*-methylpyrazine-2-carboxamide (18). A solution of $\text{SO}_2/\text{CuCl}/\text{AcOH}$ was formed by bubbling sulfur dioxide gas into acetic acid (424 mL) for 10 min at 0 °C to saturate and adding CuCl (7.15 g, 73.0 mmol). In a separate flask, an aqueous solution of NaNO_2 (25.0 g, 0.362 mol) in H_2O (380 mL) was added to a precooled (0 °C) suspension of 5-bromo-2-chloroaniline (50.0 g, 242 mol) in conc. HCl (aq., 380 mL). After stirring for 1 h, the reaction mixture was added to the $\text{SO}_2/\text{CuCl}/\text{AcOH}$ solution at 0 °C via an addition funnel over 15 min. The ice bath was removed, and the reaction mixture was allowed to stir at ambient temperature for 2 h, then diluted with H_2O (1200 mL) and filtered. The off-white solid product was concentrated in vacuo overnight to provide 63.6 g (91%) of 5-bromo-2-chlorobenzene-1-sulfonyl chloride. ^1H NMR (400 MHz, CDCl_3) δ 8.28 (d, $J = 2.3$ Hz, 1H), 7.78 (dd, $J = 8.5, 2.3$ Hz, 1H), 7.52 (d, $J = 8.5$ Hz, 1H).

A mixture of 5-bromo-2-chlorobenzene-1-sulfonyl chloride (500 mg, 1.72 mmol), *m*-toluidine (202 mg, 1.89 mmol), pyridine (1.89 mmol, 153 μL), and CH_2Cl_2 (5 mL) was stirred for 30 min then purified directly by flash chromatography (hexanes/ethyl acetate 4:1) to provide 5-bromo-2-chloro-*N*-*m*-tolylbenzenesulfonamide (521 mg, 84%) as an off-white solid.

A mixture of 5-bromo-2-chloro-*N*-*m*-tolylbenzenesulfonamide (521 mg, 1.44 mmol), bis(pinacolato)diboron (403 mg, 1.59 mmol), $\text{Pd}(\text{dppf})\text{Cl}_2\cdot\text{CH}_2\text{Cl}_2$ (105 mg, 0.129 mmol), potassium acetate (423 mg, 4.32 mmol), and dioxane (10 mL) was heated to 90 °C in a sealed tube. After 3 h, the reaction mixture was cooled to ambient temperature, and 3-amino-6-bromo-*N*-methylpyrazine-2-carboxamide (100 mg, 0.433 mmol), $\text{Pd}(\text{dppf})\text{Cl}_2\cdot\text{CH}_2\text{Cl}_2$ (42 mg, 0.051 mmol), triethylamine (238 μL , 1.84 mmol), *N,N*-dimethylformamide (2 mL), and H_2O (2 mL) were added. The reaction mixture was heated to 85 °C. After 2 h, the mixture was filtered through celite and purified directly by reverse phase HPLC (acetonitrile/aqueous ammonium acetate buffer solution; 10–90% gradient) to provide **18** (121 mg, 65% in 2 steps) as an off-white solid. ^1H NMR (400 MHz, DMSO- d_6) δ 10.60 (s, 1H), 8.83 (s, 1H), 8.79 (dd, $J = 12.0, 4.0$ Hz, 1H), 8.57 (d, $J = 2.2$ Hz, 1H), 8.41 (dd, $J = 8.4, 2.1$ Hz, 1H), 7.88 (s, 1H), 7.64–7.37 (m, 2H), 7.08 (t, $J = 7.8$ Hz, 1H), 7.02–6.88 (m, 2H), 6.79 (d, $J = 7.9$ Hz, 1H), 2.85 (d, $J = 4.8$ Hz, 3H), 2.16 (s, 3H). MS (EI) for $\text{C}_{19}\text{H}_{18}\text{ClN}_5\text{O}_3\text{S}$, found 431.8 (MH $^+$).

Compounds **7–8**, **12–14**, and **19–36** were prepared by a procedure similar to that described for the synthesis of compound **18**.

3-Amino-*N*-methyl-6-(3-(*N*-phenylsulfamoyl)phenyl)pyrazine-2-carboxamide (7). ^1H NMR (400 MHz, CD_3OD) δ 8.61 (s, 1H), 8.30–8.22 (m, 2H), 7.72–7.70 (m, 1H), 7.55 (t, $J = 7.6$ Hz, 1H), 7.24–7.20 (m, 2H), 7.12–7.04 (m, 3H), 2.97 (s, 3H). MS (EI) for $\text{C}_{18}\text{H}_{17}\text{N}_5\text{O}_3\text{S}$, found 382.1 (MH $^+$).

3-Amino-6-(4-chloro-3-(*N*-phenylsulfamoyl)phenyl)-*N*-methylpyrazine-2-carboxamide (8). ^1H NMR (400 MHz, DMSO- d_6) δ 10.69 (s, 1H), 8.84 (s, 1H), 8.79 (q, $J = 4.6$ Hz, 1H), 8.57 (d, $J = 2.4$ Hz, 1H), 8.43 (dd, $J = 8.4, 2.4$ Hz, 1H), 7.82 (br s, 2H), 7.70 (d, $J = 8.0$ Hz, 1H), 7.24–7.15 (m, 4H), 7.00–6.96 (m, 1H), 2.85 (d, $J = 5.2$ Hz, 3H). MS (EI) for $\text{C}_{18}\text{H}_{16}\text{ClN}_5\text{O}_3\text{S}$, found 418.0 (MH $^+$).

3-Amino-6-(4-methoxy-3-(*N*-phenylsulfamoyl)phenyl)-*N*-methylpyrazine-2-carboxamide (12). ^1H NMR (400 MHz, DMSO- d_6) δ 10.07 (s, 1H), 8.75 (q, $J = 4.6$ Hz, 1H), 8.73 (s, 1H), 8.35 (dd, $J = 8.4, 2.4$ Hz, 1H), 8.31 (d, $J = 2.4$ Hz, 1H), 7.63 (br s, 2H), 7.23 (d, $J = 8.8$ Hz, 1H), 7.20–7.11 (m, 4H), 6.96–6.92 (m, 1H), 3.94 (s, 3H), 2.84 (d, $J = 4.8$ Hz, 3H). MS (EI) for $\text{C}_{19}\text{H}_{19}\text{N}_5\text{O}_4\text{S}$, found 414.0 (MH $^+$).

3-Amino-6-(4-fluoro-3-(*N*-phenylsulfamoyl)phenyl)-*N*-methylpyrazine-2-carboxamide (13). ^1H NMR (400 MHz, DMSO- d_6) δ 10.68 (s, 1H), 8.83–8.79 (m, 2H), 8.50–8.47 (m, 1H), 8.41–8.37 (m, 1H), 7.78 (br s, 2H), 7.51 (t, $J = 9.2$ Hz, 1H), 7.23 (t, $J = 7.6$ Hz, 2H),

7.16 (d, $J = 7.6$ Hz, 2H), 7.01 (t, $J = 7.2$ Hz, 1H), 2.85 (d, $J = 4.8$ Hz, 3H). MS (EI) for $\text{C}_{18}\text{H}_{16}\text{FN}_5\text{O}_3\text{S}$, found 402.1 (MH $^+$).

3-Amino-6-(6-amino-5-(*N*-phenylsulfamoyl)pyridin-3-yl)-*N*-methylpyrazine-2-carboxamide (14). ^1H NMR (400 MHz, DMSO- d_6) δ 10.47 (s, 1H), 8.98 (d, $J = 2.4$ Hz, 1H), 8.76 (q, $J = 4.4$ Hz, 1H), 8.66 (s, 1H), 8.40 (d, $J = 2.4$ Hz, 1H), 7.61 (br s, 2H), 7.25–7.21 (m, 2H), 7.12 (d, $J = 7.2$ Hz, 2H), 7.00 (t, $J = 7.4$ Hz, 1H), 6.87 (s, 2H), 2.83 (d, $J = 4.4$ Hz, 3H). MS (EI) for $\text{C}_{18}\text{H}_{18}\text{N}_6\text{O}_3\text{S}$, found 400.2 (MH $^+$).

3-Amino-6-(4-chloro-3-(*N*-(3-fluorophenyl)sulfamoyl)phenyl)-*N*-methylpyrazine-2-carboxamide (19). ^1H NMR (400 MHz, DMSO- d_6) δ 11.00 (s, 1H), 8.88 (s, 1H), 8.80 (d, $J = 4.8$ Hz, 1H), 8.62 (d, $J = 2.0$ Hz, 1H), 8.46 (dd, $J = 8.4, 2.1$ Hz, 1H), 8.34–7.37 (m, 3H), 7.26 (dd, $J = 15.1, 8.1$ Hz, 1H), 7.10–6.91 (m, 2H), 6.82 (td, $J = 8.5, 1.9$ Hz, 1H), 2.86 (d, $J = 4.8$ Hz, 3H). MS (EI) for $\text{C}_{18}\text{H}_{15}\text{ClFN}_5\text{O}_3\text{S}$, found 436.0 (MH $^+$).

3-Amino-6-(4-chloro-3-(*N*-(3-methoxyphenyl)sulfamoyl)phenyl)-*N*-methylpyrazine-2-carboxamide (20). ^1H NMR (400 MHz, DMSO- d_6) δ 10.69 (s, 1H), 8.83 (s, 1H), 8.77 (dd, $J = 8.1, 4.9$ Hz, 1H), 8.58 (d, $J = 2.0$ Hz, 1H), 8.42 (d, $J = 7.8$ Hz, 1H), 8.27–7.33 (m, 3H), 7.10 (t, $J = 8.3$ Hz, 1H), 6.78–6.62 (m, 2H), 6.61–6.48 (m, 1H), 3.61 (s, 3H), 2.85 (d, $J = 4.8$ Hz, 3H). MS (EI) for $\text{C}_{19}\text{H}_{18}\text{ClN}_5\text{O}_4\text{S}$, found 448.0 (MH $^+$).

3-Amino-6-(4-chloro-3-(*N*-(3-trifluoromethyl)phenyl)sulfamoyl)phenyl)-*N*-methylpyrazine-2-carboxamide (21). ^1H NMR (400 MHz, DMSO- d_6) δ 11.18 (s, 1H), 8.86 (s, 1H), 8.80 (q, $J = 4.5$ Hz, 1H), 8.63 (d, $J = 2.2$ Hz, 1H), 8.46 (dd, $J = 8.4, 2.2$ Hz, 1H), 8.27–7.52 (m, 3H), 7.54–7.40 (m, 3H), 7.42–7.26 (m, 1H), 2.86 (d, $J = 4.8$ Hz, 3H). MS (EI) for $\text{C}_{19}\text{H}_{15}\text{ClF}_3\text{N}_5\text{O}_3\text{S}$, found 486.0 (MH $^+$).

3-Amino-6-(4-chloro-3-(*N*-(3-chlorophenyl)sulfamoyl)phenyl)-*N*-methylpyrazine-2-carboxamide (22). ^1H NMR (400 MHz, DMSO- d_6) δ 11.00 (s, 1H), 8.86 (s, 1H), 8.81 (q, $J = 4.6$ Hz, 1H), 8.62 (s, 1H), 8.46 (dd, $J = 8.4, 2.2$ Hz, 1H), 8.35–7.34 (m, 3H), 7.25–7.19 (m, 2H), 7.14 (ddd, $J = 8.2, 2.1, 0.9$ Hz, 1H), 7.05 (ddd, $J = 8.0, 2.0, 0.9$ Hz, 1H), 2.86 (d, $J = 4.8$ Hz, 3H). MS (EI) for $\text{C}_{18}\text{H}_{15}\text{Cl}_2\text{N}_5\text{O}_3\text{S}$, found 452.0 (MH $^+$).

3-Amino-6-(4-chloro-3-(*N*-(2-chlorophenyl)sulfamoyl)phenyl)-*N*-methylpyrazine-2-carboxamide (23). ^1H NMR (400 MHz, DMSO- d_6) δ 10.29 (s, 1H), 8.88–8.63 (m, 2H), 8.46 (d, $J = 10.2$ Hz, 1H), 8.41 (s, 1H), 8.12–7.55 (m, 3H), 7.43 (d, $J = 7.8$ Hz, 1H), 7.34–7.14 (m, 3H), 2.83 (d, $J = 4.8$ Hz, 3H). MS (EI) for $\text{C}_{18}\text{H}_{15}\text{Cl}_2\text{N}_5\text{O}_3\text{S}$, found 451.7 (MH $^+$).

3-Amino-6-(4-chloro-3-(*N*-(4-chlorophenyl)sulfamoyl)phenyl)-*N*-methylpyrazine-2-carboxamide (24). ^1H NMR (400 MHz, DMSO- d_6) δ 10.86 (s, 1H), 8.85 (s, 1H), 8.79 (q, $J = 4.8$ Hz, 1H), 8.57 (d, $J = 2.2$ Hz, 1H), 8.45 (dd, $J = 8.4, 2.2$ Hz, 1H), 8.30–7.43 (m, 3H), 7.28 (d, $J = 8.9$ Hz, 2H), 7.16 (d, $J = 8.9$ Hz, 2H), 2.85 (d, $J = 4.8$ Hz, 3H). MS (EI) for $\text{C}_{18}\text{H}_{15}\text{Cl}_2\text{N}_5\text{O}_3\text{S}$, found 452.0 (MH $^+$).

3-Amino-6-(3-(*N*-(3-chlorophenyl)sulfamoyl)phenyl)-*N*-methylpyrazine-2-carboxamide (25). ^1H NMR (400 MHz, CD_3OD) δ 8.65 (s, 1H), 8.35 (t, $J = 1.7$ Hz, 1H), 8.32–8.24 (m, 1H), 8.06–7.40 (m, 6H), 7.24–7.13 (m, 2H), 7.09–7.00 (m, 2H), 2.98 (s, 3H). MS (EI) for $\text{C}_{18}\text{H}_{16}\text{ClN}_5\text{O}_3\text{S}$, found 416.1 (MH $^+$).

3-Amino-6-(4-chloro-3-(*N*-(2-chloro-4-fluorophenyl)sulfamoyl)phenyl)-*N*-methylpyrazine-2-carboxamide (26). ^1H NMR (400 MHz, DMSO- d_6) δ 10.34 (s, 1H), 8.76 (s, 2H), 8.48 (d, $J = 6.2$ Hz, 1H), 8.38 (s, 1H), 7.97–7.53 (m, 3H), 7.46 (dd, $J = 8.5, 2.9$ Hz, 1H), 7.29 (dd, $J = 9.0, 5.7$ Hz, 1H), 7.22–7.14 (m, 1H), 2.83 (d, $J = 4.8$ Hz, 3H). MS (EI) for $\text{C}_{18}\text{H}_{14}\text{Cl}_2\text{FN}_5\text{O}_3\text{S}$, found 469.7 (MH $^+$).

3-Amino-6-(4-chloro-3-(*N*-(2-chloro-3-fluorophenyl)sulfamoyl)phenyl)-*N*-methylpyrazine-2-carboxamide (27). ^1H NMR (400 MHz, DMSO- d_6) δ 10.55 (s, 1H), 8.89–8.69 (m, 2H), 8.48 (dd, $J = 8.4, 2.1$ Hz, 1H), 8.45 (d, $J = 2.2$ Hz, 1H), 8.14–7.49 (m, 3H), 7.40–7.19 (m, 2H), 7.14 (d, $J = 8.0$ Hz, 1H), 2.83 (d, $J = 4.8$ Hz, 3H). MS (EI) for $\text{C}_{18}\text{H}_{14}\text{Cl}_2\text{FN}_5\text{O}_3\text{S}$, found 469.7 (MH $^+$).

3-Amino-6-(4-chloro-3-(*N*-(2-dichlorophenyl)sulfamoyl)phenyl)-*N*-methylpyrazine-2-carboxamide (28). ^1H NMR (400 MHz, DMSO- d_6) δ 10.44 (s, 1H), 8.87–8.56 (m, 2H), 8.58–8.28 (m, 2H), 7.91–7.19 (m, 6H), 2.84 (d, $J = 4.8$ Hz, 3H). MS (EI) for $\text{C}_{18}\text{H}_{14}\text{Cl}_3\text{N}_5\text{O}_3\text{S}$, found 483.7 (MH $^+$).

3-Amino-6-(4-chloro-3-(*N*-(2,3-dichlorophenyl)sulfamoyl)phenyl)-*N*-methylpyrazine-2-carboxamide (29). ^1H NMR (400 MHz, DMSO- d_6) δ 10.54 (s, 1H), 8.95–8.63 (m, 2H), 8.59–8.33 (m, 2H), 8.02–7.15 (m, 6H), 2.83 (d, J = 4.8 Hz, 3H). MS (EI) for $\text{C}_{18}\text{H}_{14}\text{Cl}_3\text{N}_5\text{O}_3\text{S}$, found 485.7 (MH^+).

3-Amino-6-(3-(*N*-(2,3-difluorophenyl)sulfamoyl)phenyl)-*N*-methylpyrazine-2-carboxamide (30). ^1H NMR (400 MHz, DMSO- d_6) δ 10.78 (s, 1H), 8.96 (s, 1H), 8.93 (q, J = 4.6 Hz, 1H), 8.45 (d, J = 2.3 Hz, 1H), 8.33 (dd, J = 8.5, 2.3 Hz, 1H), 7.97 (t, J = 2.0 Hz, 1H), 7.91–7.45 (m, 4H), 7.49–7.34 (m, 1H), 7.20 (dd, J = 7.6, 1.7 Hz, 1H), 2.84 (d, J = 4.8 Hz, 3H). MS (EI) for $\text{C}_{18}\text{H}_{15}\text{F}_2\text{N}_5\text{O}_3\text{S}$, found 419.9 (MH^+).

3-Amino-6-(4-chloro-3-(*N*-(2,3-difluorophenyl)sulfamoyl)phenyl)-*N*-methylpyrazine-2-carboxamide (31). ^1H NMR (400 MHz, DMSO- d_6) δ 10.80 (s, 1H), 8.83–8.61 (m, 2H), 8.47 (d, J = 2.2 Hz, 1H), 8.40 (d, J = 7.7 Hz, 1H), 8.24–7.36 (m, 3H), 7.15–6.85 (m, 3H), 2.84 (d, J = 4.8 Hz, 3H). MS (EI) for $\text{C}_{18}\text{H}_{14}\text{ClF}_2\text{N}_5\text{O}_3\text{S}$, found 454.0 (MH^+).

3-Amino-6-(4-chloro-3-(*N*-(3-fluoro-2-methylphenyl)sulfamoyl)phenyl)-*N*-methylpyrazine-2-carboxamide (32). ^1H NMR (400 MHz, DMSO- d_6) δ 10.15 (s, 1H), 8.86–8.63 (m, 2H), 8.48 (dd, J = 8.4, 2.3 Hz, 1H), 8.39 (d, J = 2.2 Hz, 1H), 8.11–7.30 (m, 3H), 7.11 (dd, J = 15.0, 7.9 Hz, 1H), 7.02 (t, J = 8.8 Hz, 1H), 6.85 (d, J = 7.9 Hz, 1H), 2.83 (d, J = 4.8 Hz, 3H), 2.12 (d, J = 2.1 Hz, 3H). MS (EI) for $\text{C}_{19}\text{H}_{17}\text{ClFN}_5\text{O}_3\text{S}$, found 450.0 (MH^+).

5-(5-Aminopyrazin-2-yl)-2-chloro-*N*-(2,3-difluorophenyl)benzenesulfonamide (33). ^1H NMR (400 MHz, DMSO- d_6) δ 10.76 (s, 1H), 8.57 (s, 1H), 8.49 (d, J = 2.2 Hz, 1H), 8.16 (d, J = 7.5 Hz, 1H), 7.96 (d, J = 1.4 Hz, 1H), 7.70 (d, J = 8.3 Hz, 1H), 7.20 (s, 1H), 7.15–7.01 (m, 2H), 6.81 (s, 2H). MS (EI) for $\text{C}_{16}\text{H}_{11}\text{ClF}_2\text{N}_4\text{O}_2\text{S}$, found 397.0 (MH^+).

5-(2-Aminopyrimidin-5-yl)-2-chloro-*N*-(2,3-difluorophenyl)benzenesulfonamide (34). ^1H NMR (400 MHz, DMSO- d_6) δ 8.45 (s, 2H), 8.06 (d, J = 2.3 Hz, 1H), 7.81–7.10 (m, 3H), 6.98–6.82 (m, 3H), 6.66 (dd, J = 14.0, 6.9 Hz, 1H), 6.44 (s, 1H). MS (EI) for $\text{C}_{16}\text{H}_{11}\text{ClF}_2\text{N}_4\text{O}_2\text{S}$, found 397.0 (MH^+).

5-(2-Amino-4-methoxypyrimidin-5-yl)-2-chloro-*N*-(2,3-difluorophenyl)benzenesulfonamide (35). To a stirred solution of 2-amino-4-chloropyrimidine (2.58 g, 20.0 mmol) in acetic acid (40 mL) was added dropwise bromine (1.03 mL, 20.0 mmol) at ambient temperature. After stirring for 2 h, the precipitate was collected by filtration. The yellow solid was suspended with H_2O , and the pH of the mixture was adjusted to pH 8–9 using 50% aq. NaOH. After sonication for 10 min, the precipitates were collected by filtration, washed with H_2O , and dried in vacuo to afford 2-amino-5-bromo-4-chloropyrimidine (3.59 g, 86%).

To a stirred solution of 2-amino-5-bromo-4-chloropyrimidine (627 mg, 3.00 mmol) in 1,4-dioxane (15 mL) and methanol (15 mL) was added NaOMe (4 mL of a 25 wt % solution in methanol) at ambient temperature. After stirring for 1.5 h, H_2O (20 mL) was added, and the majority of solvent was removed in vacuo. The residual aqueous layer was extracted with CH_2Cl_2 (3 \times). The combined organic layers were dried over anhydrous sodium sulfate and concentrated to provide 5-bromo-4-methoxypyrimidin-2-amine (578 mg, 94%) as a white powder. MS (EI) for $\text{C}_5\text{H}_6\text{BrN}_3\text{O}$, found 204.0 (MH^+).

Analogue 35 was synthesized using a procedure similar to that described for the synthesis of compound 18 using 5-bromo-4-methoxypyrimidin-2-amine in place of 3-amino-6-bromo-*N*-methylpyrazine-2-carboxamide. ^1H NMR (400 MHz, DMSO- d_6) δ 10.79 (s, 1H), 8.10 (s, 1H), 8.03 (d, J = 2.2 Hz, 1H), 7.74 (dd, J = 8.4, 2.2 Hz, 1H), 7.68 (d, J = 8.3 Hz, 1H), 7.31–7.18 (m, 1H), 7.18–7.05 (m, 2H), 6.91 (s, 2H), 3.80 (s, 3H). MS (EI) for $\text{C}_{17}\text{H}_{13}\text{ClF}_2\text{N}_4\text{O}_3\text{S}$, found 427.0 (MH^+).

5-(2-Amino-4-(2,2,2-trifluoroethoxy)pyrimidin-5-yl)-2-chloro-*N*-(2,3 difluorophenyl)benzenesulfonamide (36). To a stirred solution of 2-amino-5-bromo-4-chloropyrimidine (2.08 g, 9.95 mmol), 2,2,2-trifluoroethanol (2.89 mL, 40.0 mmol), and 1,4-dioxane (80 mL) was added NaH (1.6 g, 40 mmol, 60% in dispersion oil) portionwise at 0 $^\circ\text{C}$. Upon completion of the addition of NaH, the reaction mixture was allowed to stir at 80 $^\circ\text{C}$ for 2 h. The reaction mixture was cooled to ambient temperature and quenched with water

(10 mL). The organic solvent was removed in vacuo, and the aqueous layer was diluted with CH_2Cl_2 and H_2O . The separated aqueous layer was extracted with CH_2Cl_2 (2 \times), and the combined organic layers were dried over sodium sulfate, filtered, and concentrated in vacuo. The residue was purified by flash chromatography (hexanes/ethyl acetate, 3:1) to provide 5-bromo-4-(2,2,2-trifluoroethoxy)pyrimidin-2-amine (2.43 g, 89%) as an off-white powder. MS (EI) for $\text{C}_6\text{H}_5\text{BrF}_3\text{N}_3\text{O}$, found 271.9 (MH^+).

Analogue 36 was synthesized using a procedure similar to that described for the synthesis of compound 18 using 5-bromo-4-(2,2,2-trifluoroethoxy)pyrimidin-2-amine in place of 3-amino-6-bromo-*N*-methylpyrazine-2-carboxamide. ^1H NMR (400 MHz, DMSO- d_6) δ 10.75 (s, 1H), 8.23 (s, 1H), 8.10 (d, J = 2.0 Hz, 1H), 7.76–7.70 (m, 2H), 7.22–7.20 (m, 1H), 7.09–7.05 (m, 4H), 4.98 (q, J = 9.1 Hz, 2H). MS (EI) for $\text{C}_{18}\text{H}_{12}\text{ClF}_3\text{N}_4\text{O}_3\text{S}$, found 494.9 (MH^+).

Compound 9 was prepared by a procedure similar to that described for the synthesis of compound 18 using 3 equivalents of methyl amine (2 M in THF) to form the sulfonamide. 3-Amino-6-(4-chloro-3-(*N*-methylsulfamoyl)phenyl)-*N*-methylpyrazine-2-carboxamide (9): ^1H NMR (400 MHz, DMSO- d_6) δ 8.87 (s, 1H), 8.85–8.76 (m, 1H), 8.52–8.41 (m, 2H), 7.82–7.71 (m, 4H), 2.86 (d, J = 4.8 Hz, 3H), 2.54 (d, J = 4.8 Hz, 3H). MS (EI) for $\text{C}_{13}\text{H}_{14}\text{ClN}_5\text{O}_3\text{S}$, found 355.8 (MH^+).

Compound 10 was prepared by a procedure similar to that described for the synthesis of compound 18 using neat ammonium hydroxide to form the sulfonamide. 3-Amino-6-(4-chloro-3-sulfamoylphenyl)-*N*-methylpyrazine-2-carboxamide (10): ^1H NMR (400 MHz, DMSO- d_6) δ 8.87 (s, 1H), 8.83–8.73 (m, 1H), 8.58 (d, J = 2.2 Hz, 1H), 8.41 (dd, J = 8.4, 2.2 Hz, 1H), 8.28–7.23 (m, 5H), 2.86 (d, J = 4.8 Hz, 3H). MS (EI) for $\text{C}_{12}\text{H}_{12}\text{ClN}_5\text{O}_3\text{S}$, found 341.9 (MH^+).

Compound 11 was prepared by a procedure similar to that described for the synthesis of compound 18 using 3 equivalents of 2,2,2-trifluoroethylamine to form the sulfonamide. 3-Amino-6-(4-chloro-3-(*N*-(2,2,2-trifluoroethyl)sulfamoyl)phenyl)-*N*-methylpyrazine-2-carboxamide (11): ^1H NMR (400 MHz, DMSO- d_6) δ 9.01 (s, 1H), 8.88 (s, 1H), 8.85–8.76 (m, 1H), 8.54–8.39 (m, 2H), 8.09–7.42 (m, 3H), 3.90 (q, J = 9.5 Hz, 2H), 2.85 (d, J = 4.8 Hz, 3H). MS (EI) for $\text{C}_{14}\text{H}_{13}\text{ClF}_3\text{N}_5\text{O}_3\text{S}$, found 424.0 (MH^+).

Compounds 15–17 were synthesized following the reaction sequence outlined in Scheme 6 and following the procedure used to synthesize 18.

3-Amino-*N*-methyl-6-(3-(phenylsulfonamido)phenyl)pyrazine-2-carboxamide (15). ^1H NMR (400 MHz, DMSO- d_6) δ 10.40 (br s, 1H), 8.62 (q, J = 4.8 Hz, 1H), 8.59 (s, 1H), 7.83–7.79 (m, 3H), 7.68 (br s, 2H), 7.66–7.53 (m, 4H), 7.30 (t, J = 8.0 Hz, 1H), 7.08–7.05 (m, 1H), 2.85 (d, J = 5.2 Hz, 3H). MS (EI) for $\text{C}_{18}\text{H}_{17}\text{N}_5\text{O}_3\text{S}$, found 384.2 (MH^+).

3-Amino-6-(3-(3-chlorophenylsulfonamido)phenyl)-*N*-methylpyrazine-2-carboxamide (16). ^1H NMR (400 MHz, DMSO- d_6) δ 10.45 (br s, 1H), 8.65 (q, J = 4.8 Hz, 1H), 8.62 (s, 1H), 7.89–7.86 (m, 1H), 7.81 (t, J = 2.0 Hz, 1H), 7.75–7.68 (m, 3H), 7.70 (br s, 2H), 7.59 (t, J = 4.0 Hz, 1H), 7.34 (t, J = 8.0 Hz, 1H), 7.08–7.05 (m, 1H), 2.85 (d, J = 4.8 Hz, 3H). MS (EI) for $\text{C}_{18}\text{H}_{16}\text{ClN}_5\text{O}_3\text{S}$, found 416.1 (MH^+).

3-Amino-6-(4-chloro-3-(3-chlorophenylsulfonamido)phenyl)-*N*-methylpyrazine-2-carboxamide (17). ^1H NMR (400 MHz, CD_3OD) δ 8.69–8.62 (m, 1H), 8.64 (s, 1H), 8.10 (d, J = 2.4 Hz, 1H), 7.90 (dd, J = 8.8, 2.4 Hz, 1H), 7.74 (t, J = 2.0 Hz, 1H), 7.64–7.61 (m, 2H), 7.47 (t, J = 8.0 Hz, 1H), 7.40 (d, J = 8.8 Hz, 1H), 2.98 (d, J = 4.8 Hz, 3H). MS (EI) for $\text{C}_{18}\text{H}_{15}\text{Cl}_2\text{N}_5\text{O}_3\text{S}$, found 453.1 (MH^+).

PI3K Biochemical Assay. All PI3K proteins were expressed and purified in-house. Human PI3K γ with boundaries of S144-A1102 and a C-terminal His-tag was expressed in *Sf9* cells using a baculovirus expression vector system. Heterodimers of full-length N-His PI3K α , PI3K β , and PI3K δ were coexpressed with truncated p85 α [M322-N600] in the same *Sf9* expression system. Purification was done using Ni-NTA affinity columns. Protein concentration was determined by the Bradford assay, and identification was confirmed by trypsin digestion and mass spectrometry. Purity was determined by SDS-PAGE.

Enzyme activity and compound inhibition were determined using luciferase-luciferin-coupled chemiluminescence and measured as the percent of ATP consumed following the kinase reaction as described previously.⁵⁸ The standard PI3K assay buffer is composed of 50 mM Tris, pH 7.5, 1 mM EGTA, 1 mM DTT, 10 mM MgCl₂ (5 mM for PI3K γ), and 0.03% CHAPS. MgCl₂ was added only into the enzyme solution as a 2 \times concentration. The standard assay concentrations for ATP and PIP2 were 1 μ M and 10 μ M, respectively. The standard enzyme concentrations for the PI3K isoforms were PI3K α , 3 nM; PI3K β , 10 nM; PI3K δ , 4 nM; and PI3K γ , 30 nM. All reactions were conducted in 384-well white, medium binding microtiter plates. Generally, 0.5 μ L of DMSO containing varying concentrations of the test compound was mixed with 10 μ L of enzyme solution (2 \times concentration). Kinase reactions were initiated with the addition of 10 μ L of PIP2 and ATP solution (2 \times concentration). Following incubation times of 30–90 min, a 10 μ L aliquot of Promega Kinase-Glo was added and the chemiluminescence signal measured using an Envision plate reader (Perkin-Elmer). Total ATP consumption was limited to 40–60%, and IC₅₀ values of control compounds correlated well with literature references. Data are reported as the mean ($n \geq 2$).

Fixed-Cell ELISA Cellular Assay. RAW 264.7 cells (ATCC, TIB-71) were seeded at 8×10^4 cells/well onto clear bottom black 96-well tissue culture-treated plates (Corning, Costar 3904) in serum-free DMEM medium (Cellgro, 10–013-CV) one day before the assay. Dilution series of test compounds were generated using DMSO as a diluent. After resuspending diluted compounds in serum-free medium, compounds were added to the cells and incubated for 90 min. Minimal signal wells were treated with 10 μ M PI-103, a pan-PI3K inhibitor. Maximal signal wells were treated with 0.3% DMSO only. After compound treatment, cells were stimulated with 250 ng/mL Complement Factor 5a (C5a, Sigma, C5788) for 3 min. Cells were then fixed with 4% formaldehyde (Sigma, F8775) for 30 min at ambient temperature. Plates were washed four times with Tris-buffered saline (TBS; 20 mM Tris, 50 mM NaCl) containing 0.1% Triton X-100 (Sigma, T9284) using the ELx405 plate washer (BioTek), incubating with the final wash volume for 20 min at ambient temperature. The wash buffer wash was removed, to be replaced by Odyssey Blocking Buffer (Li-Cor, 927–40000). Cells were blocked for 1 h at ambient temperature. Cells were stained overnight at 4 $^{\circ}$ C on a rocker with Odyssey Blocking Buffer containing rabbit antiphospho-AKT^{S473} (1:300 dilution; Cell Signaling Technology, 4060) and mouse anti-AKT (2 μ g/mL; R&D Systems, MAB 2055) antibodies. Plates were washed four times with TBS containing 0.1% Tween-20 (Bio-Rad, 161–0781), then incubated for 1 h at ambient temperature with secondary antibodies (goat antirabbit-IRDye800CW, Li-Cor, 926–32211; goat antimouse-IRDye680, Li-Cor, 926–32220) diluted 1:400 in Odyssey Blocking Buffer containing 0.1% Tween-20. Plates were washed three times with TBS with 0.1% Tween-20, followed by two times with TBS without Tween-20, then scanned using the Odyssey detector (Li-Cor). Intrawell normalization was accomplished by dividing the phospho-AKT^{S473} intensity values from the 800 nm channel by the total AKT values from the 700 nm channel. IC₅₀ values were then estimated by comparing the values of compound-treated samples with averages of the aforementioned minimal and maximal signal condition wells. Data are reported as the mean ($n \geq 2$).

Crystallization and Structure Determination. A construct representing amino acids 114–1102 of PIK3CG was expressed in Sf-9 cells. The purification of PI3K γ protein was carried out as previously reported⁵⁹ except for the removal of betaine, ethylene glycol, and CHAPS solutes from all purification buffers. Crystals of PI3K γ were grown at 19 $^{\circ}$ C in hanging drops using vapor diffusion. The complexes were formed by incubating 49.5 μ L of PI3K γ -His₆ (7.2 mg/mL in 20 mM Tris-HCl (pH 7.2), 50 mM (NH₄)₂SO₄, and 1 mM TCEP) with 0.5 μ L of ligand (100 mM stock in 100% DMSO) for 30 min at 4 $^{\circ}$ C. Following incubation, the complexes were centrifuged at 14,000g to clarify the protein–inhibitor solutions. Crystals of the binary complexes were obtained by mixing 1.0 μ L of the PI3K γ :inhibitor complex with 1.0 μ L of a reservoir solution consisting of 16–21% PEG 4K, 0.25 M (NH₄)₂SO₄, and 0.1 M Tris-HCl (pH 7.5). In addition, 0.2 μ L of an apo-PI3K γ crystalline seed stock (1×10^{-3} dilution) was

added to the drop to aid crystal growth. Crystals generally appeared within one day and grew to full size in approximately 1–2 weeks. Crystals were transferred for 30 s into a cryoprotectant solution composed of 21% PEG 4K, 0.25 M (NH₄)₂SO₄, 0.1 M Tris-HCl (pH 7.5), 10% ethylene glycol (v/v), 10% glycerol (v/v), and 500 μ M inhibitor. The structure of the PI3K γ :inhibitor complexes were solved by molecular replacement using all protein atoms of a previous structure of PI3K γ as a search model. A single unambiguous solution was found using PHASER, with one molecule in the asymmetric unit. The resulting model was subsequently refined in REFMAC5 using rigid body and maximum likelihood procedures. At this stage, Fourier syntheses with coefficients of $F_o - F_c$ and $2F_o - F_c$ yielded clearly interpretable electron density for all atoms of the ligands. The ligands were built and minimized in Concorde/PRODRG, imported into Coot, and fit into the difference electron density. The complex was subsequently refined using maximum likelihood procedures in REFMAC5. Portions of the protein were adjusted by iterative cycles of manual rebuilding in Coot and refinement in REFMAC5, and waters were built and manually inspected in Coot.

■ ASSOCIATED CONTENT

Supporting Information

Materials and methods used in determination of pharmacokinetic, AIMCD, hERG, PgP, CYP, MDCK, and K_{sol} data. This material is available free of charge via the Internet at <http://pubs.acs.org>.

Accession Codes

PDB codes are the following: 4anv for the 1/PI3K γ complex; 4anu for the 2/PI3K γ complex; 4anx for the 4/PI3K γ complex; and 4anw for the 31/PI3K γ complex.

■ AUTHOR INFORMATION

Corresponding Author

*Exelixis, 169 Harbor Way, South San Francisco CA 94080-6109, USA. Tel: (650) 837-7006. Fax: (650) 837-8177. E-mail: hjohnson@exelixis.com.

Notes

The authors declare no competing financial interest.

■ ACKNOWLEDGMENTS

We thank Siamak Dailami for analytical support; Eun Ok Kim, Iris Ngan, Yongchang Shi, Keith Calkins, Vera Shihadeh for additional support of cell based assays; Erik Gjerstad, Arturo Picones, Lory Tan, and John Bui for collecting reported ADME data; Atulkumar Ramaiya, Ron Aoyama, and Scott Womble for obtaining PK data; Steven Richards and Amy Tshako for editorial comments.

■ ABBREVIATIONS USED

CCL5, chemokine CC motif ligand 5; CHAPS, 3-[(3-cholamidopropyl)dimethylammonio]-1-propanesulfonate; C_{max} , maximum plasma concentration; C5a, complement factor 5a; DMEM, Dulbecco's modified Eagle's medium; FACS, fluorescence-activated cell sorting; K_{sol} , kinetic solubility; MDCK, Madin–Darby canine kidney; MLM, mouse liver microsome; mTOR, mammalian target of rapamycin Pd(dppf)-Cl₂·CH₂Cl₂, [1,1' bis(diphenylphosphino)ferrocene]-dichloropalladium(II) complex with dichloromethane; PIKK, phosphoinositide kinase-related kinase; RANTES, regulated upon activation, normal T-cell expressed, and secreted; TCEP, tris(2-carboxyethyl)phosphine

■ REFERENCES

- (1) Vivanco, I.; Sawyers, C. L. The phosphatidylinositol 3-kinase AKT pathway in human cancer. *Nature Rev. Cancer* **2002**, *2*, 489–501.
- (2) Cantley, L. C. The phosphoinositide 3-kinase pathway. *Science* **2002**, *296*, 1655–1657.
- (3) Vanhaesebroeck, B.; Guillermet-Guibert, J.; Graupera, M.; Bilanges, B. The emerging mechanisms of isoform-specific PI3K signaling. *Nature Rev. Mol. Cell Biol.* **2010**, *11*, 329–341.
- (4) Vanhaesebroeck, B.; Leeyers, S. J.; Ahmadi, K.; Timms, J.; Katso, R.; Driscoll, P. C.; Woscholski, R.; Parker, P. J.; Waterfield, M. D. Synthesis and function of 3-phosphorylated inositol lipids. *Annu. Rev. Biochem.* **2001**, *70*, 535–602.
- (5) Fruman, D. A.; Meyers, R. E.; Cantley, L. C. Phosphoinositide kinases. *Annu. Rev. Biochem.* **1998**, *67*, 481–507.
- (6) Krugmann, S.; Hawkins, P. T.; Pryer, N.; Braselmann, S. Characterizing the interactions between the two subunits of the p101/p110 γ phosphoinositide 3-kinase and their role in the activation of this enzyme by G $\beta\gamma$ subunits. *J. Biol. Chem.* **1999**, *274*, 17152–17158.
- (7) Stephens, L.; Smrcka, A.; Cooke, F. T.; Jackson, T. R.; Sternweis, P. C.; Hawkins, P. T. A novel phosphoinositide 3 kinase activity in myeloid-derived cells is activated by G-protein $\beta\gamma$ subunits. *Cell* **1994**, *77*, 83–93.
- (8) Stoyanov, B.; Volinia, S.; Hanck, T.; Rubio, I.; Loubtchenkov, M.; Malek, D.; Stoyanova, S.; Vanhaesebroeck, B.; Dhand, R.; Nurnberg, B.; Gierschik, P.; Seedorf, K.; Hsuan, J. J.; Waterfield, M. D.; Wetzker, R. Cloning and characterization of a G-protein activated human phosphoinositide 3-kinase. *Science* **1995**, *269*, 690–693.
- (9) Stephens, L. R.; Eguinoa, A.; Erdjument-Bromage, H.; Lui, M.; Cooke, F.; Coadwell, J.; Smrcka, A. S.; Thelen, M.; Cadwallader, K.; Tempst, P.; Hawkins, P. T. The G $\beta\gamma$ sensitivity of a PI3K is dependent upon a tightly associated adaptor, p101. *Cell* **1997**, *89*, 105–114.
- (10) Okkenhaug, K.; Vanhaesebroeck, B. PI3K in lymphocyte development, differentiation, and activation. *Nature Rev. Immunol.* **2003**, *3*, 317–330.
- (11) Wetzker, R.; Rommel, C. Phosphoinositide 3-kinases as targets for therapeutic intervention. *Curr. Pharm. Des.* **2004**, *10*, 1915–1922.
- (12) Foukas, L. C.; Claret, M.; Pearce, W.; Okkenhaug, K.; Meek, S.; Peskett, E.; Sancho, S.; Smith, A. J. H.; Withers, D. J.; Vanhaesebroeck, B. Critical role for the p110 α phosphoinositide-3-OH kinase in growth and metabolic regulation. *Nature* **2006**, *441*, 366–370.
- (13) Samuels, Y.; Wang, Z.; Bardelli, A.; Silliman, N.; Ptak, J.; Szabo, S.; Yan, H.; Gazdar, A.; Powell, S. M.; Riggins, G. J.; Willson, J. K.; Markowitz, S.; Kinzler, K. W.; Vogelstein, B.; Velculescu, V. E. High frequency of mutations of the *PIK3Ca* gene in human cancers. *Science* **2004**, *304*, 554.
- (14) Ghigo, A.; Damilano, F.; Braccini, L.; Hirsch, E. PI3K inhibition in inflammation: Toward tailored therapies for specific diseases. *BioEssays* **2010**, *32*, 185–196.
- (15) Reif, K.; Okkenhaug, K.; Sasaki, T.; Penninger, J. M.; Vanhaesebroeck, B.; Cyster, J. G. Differential roles for phosphoinositide 3-kinases, p110 γ and p110 δ , in lymphocyte chemotaxis and homing. *J. Immunol.* **2004**, *173*, 2236–2240.
- (16) Laffargue, M.; Calvez, R.; Finan, P.; Trifilieff, A.; Barbier, M.; Altruda, F.; Hirsch, E.; Wymann, M. P. Phosphoinositide 3-kinase γ is an essential amplifier of mast cell function. *Immunity* **2002**, *16*, 441–451.
- (17) Martin, D.; Galisteo, R.; Molinolo, A. A.; Wetzker, R.; Hirsch, E.; Gutkind, J. S. PI3K γ mediates kaposi's sarcoma-associated herpesvirus vGPCR-induced sarcomagenesis. *Cancer Cell* **2011**, *19*, 805–813.
- (18) Schmid, M. C.; Avraamides, C. J.; Dippold, H. C.; Franco, I.; Foubert, P.; Ellies, L. G.; Acevedo, L. M.; Manglicmot, J. R. E.; Song, X.; Wrasidlo, W.; Blair, S. L.; Ginsberg, M. H.; Cheresch, D. A.; Hirsch, E.; Field, S. J.; Varner, J. A. Receptor tyrosine kinases and TLR/IL1Rs unexpectedly activate myeloid cell PI3K γ , a single convergent point promoting tumor inflammation and progression. *Cancer Cell* **2011**, *19*, 715–727.
- (19) Gonzalez-Garcia, A.; Sanchez-Ruiz, J.; Flores, J. M.; Carrera, A. C. Phosphatidylinositol 3-kinase γ inhibition ameliorates inflammation and tumor growth in a model of colitis-associated cancer. *Gastroenterology* **2010**, *138*, 1374–1383.
- (20) Monterrubio, M.; Mellado, M.; Carrera, A. C.; Rodriguez-Frade, J. M. R.-F. PI3K γ activation by CXCL12 regulates tumor cell adhesion and invasion. *Biochem. Biophys. Res. Commun.* **2009**, *388*, 199–204.
- (21) Attoub, S.; De Wever, O.; Bruyneel, E.; Mareel, M.; Gespach, C. The transforming functions of PI3-kinase- γ are linked to disruption of intercellular adhesion and promotion of cancer cell invasion. *Ann. N.Y. Acad. Sci.* **2008**, *1138*, 204–213.
- (22) Kobayashi, N.; Ueki, K.; Okazaki, Y.; Iwane, A.; Kubota, N.; Ohsugi, M.; Awazaw, M.; Kobayashi, M.; Sasako, T.; Kaneko, K.; Suzuki, M.; Nishikawa, Y.; Hara, K.; Yoshimura, K.; Koshima, I.; Goyama, S.; Murakami, K.; Sasaki, J.; Nagai, R.; Kurokawa, M.; Sasaki, T.; Kadowaki, A. Blockade of class IB phosphoinositide-3 kinase ameliorates obesity-induced inflammation and insulin resistance. *Proc. Natl. Acad. Sci. U.S.A.* **2011**, *108*, 5753–5758.
- (23) Damilano, F.; Franco, I.; Perrino, C.; Schaefer, K.; Azzolino, O.; Carnevale, D.; Cifelli, G.; Carullo, P.; Ragona, R.; Ghigo, A.; Perino, A.; Lembo, G.; Hirsch, E. Distinct effects of leukocyte and cardiac phosphoinositide 3-kinase γ activity in pressure overload-induced cardiac failure. *Circulation* **2001**, *123*, 391–399.
- (24) Jin, R.; Song, Z.; Yu, S.; Piazza, A.; Nanda, A.; Penninger, J. M.; Granger, D. N.; Li, G. Phosphatidylinositol-3-kinase gamma plays a central role in blood-brain barrier dysfunction in acute experimental stroke. *Stroke* **2011**, *42*, 2033–2044.
- (25) Guo, D.; Thiyam, G.; Bodiga, S.; Kassiri, Z.; Oudit, G. Y. Uncoupling between enhanced excitation-contraction coupling and the response to heart disease: Lessons from the PI3K γ knockout murine model. *J. Mol. Cell Cardiol.* **2011**, *50*, 606–612.
- (26) Siragusa, M.; Katare, R.; Meloni, M.; Damilano, F.; Hirsch, E.; Emanuelli, C.; Madeddu, P. Involvement of phosphoinositide kinase γ in angiogenesis and healing of experimental myocardial infarction in mice. *Circ. Res.* **2010**, *106*, 757–768.
- (27) Seropian, I. M.; Abbate, A.; Toldo, S.; Harrington, J.; Smithson, L.; Ockaili, R.; Mezzaroma, E.; Damilano, F.; Hirsch, E.; Van Tassel, B. W. Pharmacologic inhibition of phosphoinositide 3-kinase gamma (PI3K γ) promotes infarct resorption and prevents adverse cardiac remodeling after myocardial infarction in mice. *J. Cardiovasc. Pharm.* **2010**, *56*, 651–658.
- (28) Jin, R.; Yu, S.; Song, Z.; Quillin, J. W.; Deasis, D. P.; Penninger, J. M.; Nanda, A.; Granger, D. N.; Li, G. Phosphoinositide 3-kinase-gamma expression is upregulated in brain microglia and contributes to ischemia-induced microglial activation in acute experimental stroke. *Biochem. Biophys. Res. Commun.* **2010**, *399*, 458–464.
- (29) Passos, G. F.; Figueiredo, C. P.; Prediger, R. D. S.; Silva, K. A. B. S.; Siqueira, J. M.; Duarte, F. S.; Leal, P. C.; Medeiros, R.; Calixto, J. B. Involvement of phosphoinositide 3-kinase γ in the neuro-inflammatory response and cognitive impairments induced by β -amyloid 1–40 peptide in mice. *Brain Behav. Immun.* **2010**, *24*, 493–501.
- (30) Maira, S. M.; Finan, P.; Garcia-Echeverria, C. From the bench to the bed side: PI3K pathway inhibitors in clinical development. *Curr. Top. Microbiol. Immunol.* **2011**, *347*, 209–239.
- (31) Shapiro, G.; Kwak, E.; Baselga, J.; Rodon, J.; Scheffold, C.; Laird, A. D.; Bedell, C.; Edelman, G. Phase I dose-escalation study of XL147, a PI3K inhibitor administered orally to patients with solid tumors. Presented at ASCO 2009 Annual Meeting, Orlando, FL, May 29–June 2, 2009; Abstract 3500
- (32) Papadopoulos, K. P.; Markman, B.; Taberner, J.; Patnaik, A.; Heath, E. I.; DeCillis, A.; Laird, D.; Aggarwal, S. K.; Nguyen, L.; LoRusso, P. M. A phase I dose-escalation study of the safety, pharmacokinetics (PK), and pharmacodynamics (PD) of a novel PI3K inhibitor, XL765, administered orally to patients (pts) with advanced solid tumors. Presented at ASCO 2009 Annual Meeting, Chicago, IL, May 30–June 3, 2008; Abstract 3510
- (33) Rückle, T.; Schwarz, M. K.; Rommel, C. PI3K γ inhibition: towards an 'aspirin of the 21st century'? *Nat. Rev. Drug Discovery* **2006**, *5*, 903–918.

- (34) Rommel, C.; Camps, M.; Ji, H. PI3K δ and PI3K γ : partners in crime in inflammation in rheumatoid arthritis and beyond? *Nat. Rev. Drug Discovery* **2007**, *7*, 191–201.
- (35) Ameriks, M. K.; Venable, J. D. Small Molecule inhibitors of phosphoinositide 3-kinase (PI3K) δ and γ . *Curr. Top. Med. Chem.* **2009**, *9*, 738–753.
- (36) Pacold, M. E.; Suire, S.; Perisic, O.; Lara-Gonzalez, S.; Davis, C. T.; Walker, E. H.; Hawkins, P. T.; Stephens, L.; Eccleston, J. F.; Williams, R. L. Crystal structure and functional analysis of Ras binding to its effector phosphoinositide 3-kinase γ . *Cell* **2000**, *103*, 931–943.
- (37) Suire, S.; Hawkins, P.; Stephens, L. Activation of phosphoinositide 3-kinase γ by Ras. *Curr. Biol.* **2002**, *12*, 1068–1075.
- (38) Bondeva, T.; Pirola, L.; Bulgarelli-Leva, G.; Rubio, I.; Wetzker, R.; Wymann, M. P. Bifurcation of lipid and protein kinase signals of PI3K γ to the protein kinases PKB and MAPK. *Science* **1998**, *282*, 293–296.
- (39) Lopez-Illasaca, M.; Gutkind, J. S.; Wetzker, R. Phosphoinositide 3-kinase γ is a mediator of G $\beta\gamma$ -dependent Jun kinase activation. *J. Biol. Chem.* **1998**, *273*, 2505–2508.
- (40) Li, Z.; Jiang, H.; Xie, W.; Zhang, Z.; Smrcka, A. V.; Wu, D. Roles of PLC- β 2 and - β 3 and PI3K γ in chemoattractant-mediated signal transduction. *Science* **2000**, *287*, 1046–1049.
- (41) Hirsch, E.; Katanaev, V. L.; Garlanda, C.; Azzolino, O.; Pirola, L.; Silengo, L.; Sozzani, S.; Mantovani, A.; Altruda, F.; Wymann, M. P. Central role for G protein-coupled phosphoinositide 3-kinase γ in inflammation. *Science* **2000**, *287*, 1049–1053.
- (42) Sasaki, T.; Irie-Sasaki, J.; Jones, R. G.; Oliveira-dos-Santos, A. J.; Stanford, W. L.; Bolon, B.; Wakeham, A.; Itie, A.; Bouchard, D.; Kozieradzki, L.; Joza, J.; Mak, T. W.; Ohashi, P. S.; Suzuki, A.; Penninger, J. M. Function of PI3K γ in thymocyte development, T cell activation, and neutrophil migration. *Science* **2000**, *287*, 1040–1046.
- (43) Camps, M.; Rückle, T.; Ji, H.; Ardisson, V.; Rintelen, F.; Shaw, J.; Ferrandi, C.; Chabert, C.; Gillieron, C.; Françon, B.; Martin, T.; Gretener, D.; Perrin, D.; Leroy, D.; Vitte, P. A.; Hirsch, E.; Wymann, M. P.; Cirillo, R.; Schwarz, M. K.; Rommel, C. Blockade of PI3K γ suppresses joint inflammation and damage in a murine model of rheumatoid arthritis. *Nature Med.* **2005**, *11*, 936–943.
- (44) Pomel, V.; Klicic, J.; Covini, D.; Church, D. D.; Shaw, J. P.; Roulin, K.; Burgat-Charvillon, F.; Valognes, D.; Camps, M.; Chabert, C.; Gillieron, C.; Françon, B.; Perrin, D.; Leroy, D.; Gretener, D.; Nichols, A.; Vitte, P. A.; Carboni, S.; Rommel, C.; Schwarz, M. K.; Rückle, T. Furan-2-ylmethylene thiazolidinediones as novel, potent, and selective inhibitors of phosphoinositide 3-kinase γ . *J. Med. Chem.* **2006**, *49*, 3857–3871.
- (45) Buhr, C. A.; Baik, T.-G.; Sunghoon, M.; Tesfai, Z.; Wang, L.; Co, E. W.; Epshteyn, S.; Kennedy, A. R.; Chen, B.; Dubenko, L.; Anand, N. K.; Tsang, T. H.; Nuss, J. M.; Peto, C. J.; Rice, K. D.; Ibrahim, M. A.; Schnepf, K. L.; Shi, X.; Leahy, J. W.; Chen, J.; Dalrymple, L. E.; Forsyth, T. P.; Huynh, T. P.; Mann, G.; Mann, L. W.; Takeuchi, C. S.; Lamb, P.; Matthews, D. J.; Miller, N. Protein Kinase Modulators and Methods of Use. PCT Int. Appl. WO0309329A2, 2003.
- (46) Sundstrom, T. J.; Anderson, A. C.; Wright, D. L. Inhibitors of phosphoinositide-3-kinase: a structure-based approach to understanding potency and selectivity. *Org. Biomol. Chem.* **2009**, *7*, 840–850.
- (47) Walker, E. H.; Perisic, O.; Ried, C.; Stephens, L.; Williams, R. L. Structural insights into phosphoinositide 3-kinase catalysis and signalling. *Nature* **1999**, *402*, 313–320.
- (48) Calculated using ACD Laboratories software 9.0.
- (49) Mouse plasma exposure of **11**: 44.4 ± 14.3 and 17.9 ± 3.5 μ M in plasma at 1 and 4 h. respectively. dosed in male BALB/c mice ($n = 3$) at 100 mpk as a solution in 10% EtOH 60% PEG400/water.
- (50) Ali, K.; Camps, M.; Pearce, W. P.; Ji, H.; Kuehn, N.; Pasquali, C.; Chabert, C.; Rommel, C.; Vanhaesebroeck, B. Isoform-specific functions of phosphoinositide 3-kinases: p110 δ but not p110 γ promotes optimal allergic responses in vivo. *J. Immunol.* **2008**, *180*, 2538–2544.
- (51) Folkes, A. J.; Ahmadi, K.; Alderton, W. K.; Alix, S.; Baker, S. J.; Box, G.; Chuckowree, I. S.; Clarke, P. A.; Depledge, P.; Eccles, S. A.; Friedman, L. S.; Hayes, A.; Hancox, T. C.; Kugendradas, A.; Lensun, L.; Moore, P.; Olivero, A. G.; Pang, J.; Patel, S.; Pergl-Wilson, G. H.; Raynaud, F. I.; Robson, A.; Saghir, N.; Salphati, L.; Sohal, S.; Ultsch, M. H.; Valenti, M.; Wallweber, H. J.; Wan, N. C.; Wiesmann, C.; Workman, P.; Zhyvoloup, A.; Zvebil, M. J.; Shuttleworth, S. J. The Identification of 2-(1H-indazol-4-yl)-6-(4-methanesulfonyl-piperazin-1-ylmethyl)-4-morpholin-4-yl-thieno[3,2-d]pyrimidine (GDC-0941) as a potent, selective, orally bioavailable inhibitor of class I PI3 kinase for the treatment of cancer. *J. Med. Chem.* **2008**, *51*, 5522–5532.
- (52) Gendreau, S. B.; Ventura, R.; Keast, P.; Laird, A. D.; Yakes, F. M.; Zhang, W.; Bentzien, F.; Cancilla, B.; Lutman, J.; Chu, F.; Jackman, L.; Shi, Y.; Yu, P.; Wang, J.; Aftab, A. T.; Jaeger, C. T.; Meyer, S. M.; De Costa, A.; Engell, K.; Chen, J.; Martini, J. F.; Joly, A. H. Inhibition of the T790M gatekeeper mutant of the epidermal growth factor receptor by EXEL-7647. *Clin. Cancer Res.* **2007**, *13*, 3713–3723.
- (53) Qian, F.; Engst, S.; Yamaguchi, K.; Yu, P.; Won, K. A.; Mock, L.; Lou, T.; Tan, J.; Li, C.; Tam, D.; Lougheed, J.; Yakes, M. F.; Bentzien, F.; Xu, W.; Zaks, T.; Wooster, R.; Greshock, J.; Joly, A. H. Inhibition of tumor cell growth, invasion, and metastasis by EXEL-2880 (XL880, GSK1363089), a novel inhibitor of HGF and VEGF receptor tyrosine kinases. *Cancer Res.* **2009**, *69*, 8009–8016.
- (54) Zoncu, R.; Efayan, A.; Sabatini, D. M. mTOR: from growth signal integration to cancer, diabetes and ageing. *Nature Rev. Mol. Cell Biol.* **2011**, *12*, 21–35.
- (55) Adams, N. D.; Burgess, J. L.; Darcy, M. G.; Donatelli, C. A.; Knight, S. D.; Newlander, K. A.; Ridgers, L.; Sarpong, M.; Schmidt, S. J. Preparation of Quinoline Derivatives as PI3 Kinase Inhibitors. PCT Int. Appl. WO144463A1, 2008.
- (56) Harris, K. J.; Lang, H.-J.; Mathew, R. M.; Shimshock, S. J.; Nieduzak, T. R.; Jackson, S.; Yang, Z.; Bordeau, K. J. 2-Phenyl-indoles as Prostaglandin D2 Receptor Antagonists. PCT Int. Appl. WO2006081343, 2006.
- (57) Ibrahim, M. A.; Johnson, H. W. B.; Jeong, J. W.; Lewis, G. L.; Shi, X.; Noguchi, R. T.; Williams, M.; Leahy, J. W.; Nuss, J. M.; Woolfrey, J.; Banica, M.; Bentzien, F.; Chou, Y.-C.; Gibson, A.; Heald, N.; Lamb, P.; Mattheakis, L.; Matthews, D.; Shipway, A.; Wu, X.; Zhang, W.; Zhou, S.; Shankar, G. Discovery of a novel class of potent and orally bioavailable sphingosine 1-phosphate receptor 1 antagonists. *J. Med. Chem.* **2012**, *55*, 1368–1381.
- (58) Munagala, N.; Nguyen, S.; Lam, W.; Lee, J.; Joly, A.; McMillan, K.; Zhang, W. Identification of small molecule ceramide kinase inhibitors using a homogeneous chemiluminescence high throughput assay. *Assay Drug Dev. Technol.* **2007**, *5*, 65–73.
- (59) Walker, E. H.; Pacold, M. E.; Perisic, O.; Stephens, L.; Hawkins, P. T.; Wymann, M. P.; Williams, R. L. Structural determinants of phosphoinositide 3-kinase inhibition by wortmannin, LY294002, quercetin, myricetin, and staurosporine. *Mol. Cell* **2000**, *6*, 909–919.